

Cardiac metabolic effects of $K_{Na}1.2$ channel deletion and evidence for its mitochondrial localization

Charles O. Smith,* Yves T. Wang,[†] Sergiy M. Nadtochiy,[†] James H. Miller,[†] Elizabeth A. Jonas,[‡] Robert T. Dirksen,[§] Keith Nehrke,^{§,¶} and Paul S. Brookes^{†,§,1}

*Department of Biochemistry, [†]Department of Anesthesiology and Perioperative Medicine, [§]Department of Pharmacology and Physiology, and [¶]Department of Medicine, University of Rochester Medical Center, Rochester, New York, USA; and [‡]Section of Endocrinology, Department of Internal Medicine, Yale University School of Medicine, New Haven, Connecticut, USA

ABSTRACT: Controversy surrounds the molecular identity of mitochondrial K^+ channels that are important for protection against cardiac ischemia–reperfusion injury. Although $K_{Na}1.2$ (sodium-activated potassium channel encoded by *Kcnt2*) is necessary for cardioprotection by volatile anesthetics, electrophysiological evidence for a channel of this type in mitochondria is lacking. The endogenous physiological role of a potential mito- $K_{Na}1.2$ channel is also unclear. In this study, single channel patch clamp of 27 independent cardiac mitochondrial inner membrane (mitoplast) preparations from wild-type (WT) mice yielded 6 channels matching the known ion sensitivity, ion selectivity, pharmacology, and conductance properties of $K_{Na}1.2$ (slope conductance, 138 ± 1 pS). However, similar experiments on 40 preparations from *Kcnt2*^{-/-} mice yielded no such channels. The K_{Na} opener bithionol uncoupled respiration in WT but not *Kcnt2*^{-/-} cardiomyocytes. Furthermore, when oxidizing only fat as substrate, *Kcnt2*^{-/-} cardiomyocytes and hearts were less responsive to increases in energetic demand. *Kcnt2*^{-/-} mice also had elevated body fat, but no baseline differences in the cardiac metabolome. These data support the existence of a cardiac mitochondrial $K_{Na}1.2$ channel, and a role for cardiac $K_{Na}1.2$ in regulating metabolism under conditions of high energetic demand.—Smith, C. O., Wang, Y. T., Nadtochiy, S. M., Miller, J. H., Jonas, E. A., Dirksen, R. T., Nehrke, K., Brookes, P. S. Cardiac metabolic effects of $K_{Na}1.2$ channel deletion and evidence for its mitochondrial localization. *FASEB J.* 32, 6135–6149 (2018). www.fasebj.org

KEY WORDS: patch clamp · Slick · Slo2.1 · bithionol

Numerous strategies for protection of the heart and other organs against ischemia–reperfusion (IR) injury are thought to require activation of K^+ channels in the mitochondrial inner membrane [for a review, see Smith *et al.* (1)], including ischemic preconditioning, volatile anesthetic preconditioning (APC), and pharmacologic cardioprotection by K^+ channel activators, such as NS-11021, bithionol (BT), and diazoxide (2–4). Concurrently, several K^+ channels have been reported in mitochondria, including ATP-activated (K_{ATP}) (5), small-conductance

Ca^{2+} -activated (SK) (6, 7), and splice variants of large-conductance Ca^{2+} activated (BK) (8, 9). However, in only a small number of cases has the molecular (genetic) identity of specific mitochondrial channels involved in cardioprotection been proposed (3, 9–12). There are no K^+ channels in the MitoCarta database of verified mitochondrial proteins (13), and no canonical mitochondrial target sequences have been identified in any K^+ channel genes (1). As such, no clear mechanisms are known for the K^+ channel targeting to mitochondria.

Mammalian sodium-activated potassium (K_{Na}) channels are encoded by 2 genes: *Kcnt1* ($K_{Na}1.1$; Slick/SLO2.2) (14) and *Kcnt2* ($K_{Na}1.2$; Slick/SLO2.1) (15). Both $K_{Na}1.1$ and $K_{Na}1.2$ channels play important neurologic roles in the termination of seizure progression in epilepsy (16, 17). Although $K_{Na}1.2$ expression has been reported in cardiac tissue (15, 18) and a generic K_{Na} channel activity has been demonstrated in the cardiac cell membrane (19), notably the *Kcnt2*^{-/-} mice have no cardiac phenotype (3, 18). Thus relatively little is known regarding the physiological role of $K_{Na}1.2$ channels in the heart, including their subcellular location. In an earlier study, we showed that $K_{Na}1.2$ is essential for cardiac APC, with hearts from *Kcnt2*^{-/-} mice incapable of being protected against IR injury by isoflurane

ABBREVIATIONS: APC, anesthetic preconditioning; BDM, 2,3-butanedione monoxime; BT, bithionol; DEXA, dual-energy X-ray absorptiometry; FCCP, carbonylcyanide-*p*-trifluoromethoxyphenylhydrazone; HEPES, 4-(2-hydroxyethyl)-1-piperazineethanesulfonic acid; IPC, ischemic preconditioning; IR, ischemia–reperfusion; K_{Na} , sodium-activated potassium; KH, Krebs-Henseleit; MIM, mitochondrial isolation medium; MS/MS, tandem mass spectrometry; NCLX, Na^+/Ca^{2+} exchanger; OCR, oxygen consumption rate; qPCR, quantitative PCR; ROS, reactive oxygen species; RR, respiratory reserve; SDHA, succinate dehydrogenase complex, subunit A; Slick, $K_{Na}1.1$ (formerly Slo2.2; aka KCa4.1); Slick, $K_{Na}1.2$ (formerly Slo2.1; aka KCa4.2); WT, wild type; XF, extracellular flux

¹ Correspondence: Department of Anesthesiology, University of Rochester Medical Center, 601 Elmwood Ave., Box 604, Rochester, NY 14642, USA. E-mail: paul_brookes@urmc.rochester.edu

doi: 10.1096/fj.201800139R

(3). In addition, we showed that the K_{Na} opener BT is cardioprotective in wild-type (WT) mice but not in $Kcnt2^{-/-}$ mice (3, 20). Further, both BT and isoflurane activated a K^+ flux in cardiac mitochondria isolated from WT mice but not in those from $Kcnt2^{-/-}$ mice (3). These observations led us to hypothesize that there are $K_{Na}1.2$ channels in cardiac mitochondria.

There is considerable evidence that mitochondrial K^+ channel activity can lessen the impact of IR injury (1). Less is known about the endogenous physiological roles of mitochondrial K^+ channels (21)—in particular, mitochondrial K_{Na} channels. Na^+ enters mitochondria predominantly *via* an Na^+/Ca^{2+} exchanger (NCLX) or an $Na^+/monocarboxylate$ transporter (MCT), with minor contribution from an Na^+/H^+ exchanger (22). Under conditions of elevated mitochondrial Na^+ uptake (Ca^{2+} overload or cytosolic Na^+ overload driving excessive NCLX activity or increased cytosolic Na^+ -lactate driving Na^+ uptake *via* the $Na^+/monocarboxylate$ transporter), matrix Na^+ may attain levels that can activate K_{Na} channels (22–24). K^+ influx *via* the K_{Na} would dissipate mitochondrial membrane potential, thereby relieving a driving force for both Ca^{2+} uptake and NCLX activity. In effect, a mitochondrial K_{Na} channel would be predicted to act as a safety valve to prevent ionic imbalance brought about by excessive Na^+ uptake.

Using electrophysiological techniques (mitoplast patch clamp), we demonstrated that mitochondria contain a K^+ channel that matches the known ion sensitivity, ion selectivity, pharmacology, and conductance properties of $K_{Na}1.2$. Bioenergetic studies of WT and $Kcnt2^{-/-}$ hearts and cardiomyocytes also revealed a potential role for cardiac $K_{Na}1.2$ in the metabolic response to a high energy demand.

MATERIALS AND METHODS

Animals

Male and female mice were housed in an Association for Assessment and Accreditation of Laboratory Animal Care–accredited pathogen-free facility with water and food available *ad libitum*. All procedures were locally approved and in accordance with the *Guide for the Care and Use of Laboratory Animals* [National Institutes of Health (NIH), Bethesda, MD, USA]. Mice were on a C57BL/6J background for >6 generations and periodically backcrossed to fresh stocks. Mice were bred from $Kcnt2^{+/-}$ parents, and male and females were separated, but otherwise littermate WT and $Kcnt2^{-/-}$ progeny were maintained in the same cages. Mice were genotyped by tail-clip PCR (Fig. 1A), with DNA extraction by a DNeasy Kit (Qiagen, Hilden, Germany) and genotyping by a KAPA2G Kit (Kapa Biosystems, Wilmington, MA, USA). Primers used were (5'→3') forward-5'-AGGCAGCCATAGCTTTAGAGA-3' and reverse 5'-CTCCTCATCGTGTGGTCTA-3', yielding amplicons at 822 and 547 bp for WT and $Kcnt2^{-/-}$ samples, respectively. Male and female mice were used for the experiments, and data are reported for the sexes separately or combined. Because the same personnel handled the mice and performed the experiments, the studies were not blinded to genotype.

Patch-clamp assessment of mitochondrial inner membranes

After anesthesia (tribromoethanol 200 mg/kg, i.p.), the heart from each 8–12-wk-old mouse was rapidly excised, washed, and

chopped in ice-cold mitochondrial isolation medium [MIM, mM: 300 sucrose, 20 Tris, and 2 EGTA (pH 7.35)] at 4°C. All steps were performed on ice. Tissue was homogenized (Tissumizer; IKA, Inc., Wilmington, NC, USA) then centrifuged at 700 g, 5 min. Supernatants were saved and pellets rehomogenized and recentrifuged. Pooled supernatants were then centrifuged at 10,000 g for 10 min. The crude mitochondrial pellet was suspended in 0.2 ml MIM and layered over 1.75 ml of 30% osmotically balanced Percoll (MilliporeSigma, Burlington, MA, USA), in a round-bottomed microcentrifuge tube and centrifuged at 14,000 g for 1 h. Two mitochondrial layers were apparent (Fig. 1C), of which the lower (purified mitochondria) was washed twice by centrifugation. The mitochondrial pellet (~25 μ l) was suspended in 0.5 ml swelling buffer [mM: 30 KCl, 20 [4-(2-hydroxyethyl)-1-piperazineethanesulfonic acid (HEPES), and 1 EGTA, (pH 7.2)] for 15 min. Centrifugation (1000 g, 30 s) afforded a mitoplast pellet, resuspended in ~20 μ l MIM for immediate use in patch-clamp studies ($n = 27$ WT and 40 $Kcnt2^{-/-}$ mice).

For attached mitochondrial inner membrane (mitoplast) patch-clamp experiments, mitochondrial inner membranes (mitoplasts) were diluted 1:100 in a bath solution [mM: 150 KCl, 20 HEPES, 1 EGTA (pH 7.2)], and a 10- μ l drop was placed on a glass coverslip attached to a custom 3-dimensional printed microchamber (Fig. 1B) (the stereolithography file is deposited at <https://3dprint.nih.gov/discover/3dpx-008253>). Electrodes (40–100 M Ω) (Sutter Instruments, Novato, CA, USA) were filled with a pipette solution [mM: 150 KCl, 0.025 NaCl, 20 HEPES, and 1 EGTA (pH 7.2)]. The bath was exchanged with buffer additionally containing 40 mM NaCl or 40 mM NaCl with 10 μ M BT (from stock in DMSO, final DMSO concentration, <0.01% v/v). For excised patch experiments, mitoplasts were diluted 1:100 in patch seal buffer [mM: 60 KCl, 80 K-gluconate, 40 LiCl, 0.025 NaCl, 0.1 CaCl₂ [calculated free], 20 HEPES, and 1 EGTA (pH 7.2)]. Electrodes were filled with pipette solution (mM: 125 KCl, 15 K-gluconate, 15 LiCl 0.025 NaCl, 20 HEPES, and 1 EGTA). Mitoplasts were identified by their round shape and the presence of a cap structure (Fig. 1C). After formation of high-resistance seals, patches were excised and inside-out currents were recorded with an Axopatch 200B amplifier and Clampex10 software (Molecular Devices, Sunnyvale, CA, USA). All holding potentials reported are those applied to the patch pipette interior. The electrical connection was made using Ag/AgCl electrodes and an agar 2 M KCl salt bridge at the ground electrode. (Not all channels yielded currents at all potentials, and seal integrity was often compromised at the extremes of this range). Data were digitized and recorded at 10 kHz and filtered through an 8-pole low-pass 2 kHz filter. Patches were recorded under flow (0.1 ml/min) of: 1) Ca^{2+} free patch seal buffer with 0.076 mM sucrose for osmotic balance as above; 2) with LiCl replaced with 40 mM NaCl; and 3) further addition of 2.5 μ M BT (from stock in DMSO, final DMSO concentration, <0.01% v/v). Although the study of K^+ channels typically employs gluconate salts to exclude the possibility that measured conductances are related to Cl^- channels, we used Cl^- salts in this study because $K_{Na}1.2$ activity is strongly enhanced in the presence of Cl^- (15). All buffers were filtered (0.22 μ m) immediately before use. Single channel analysis was performed with a Clampfit 10.0 single-channel search (Molecular Devices). Dwell times were calculated with the single-channel search with threshold crossing.

Cardiomyocyte isolation and respiration measurements

Primary adult ventricular cardiomyocytes from male and female mice were isolated by collagenase perfusion in the presence of 10 mM 2,3-butanedione monoxime (BDM), as we previously described (3). BDM was absent from all subsequent steps. Cells were step-wise rendered tolerant to 1.8 mM Ca^{2+} , and the final pellet suspended in 1 ml MEM

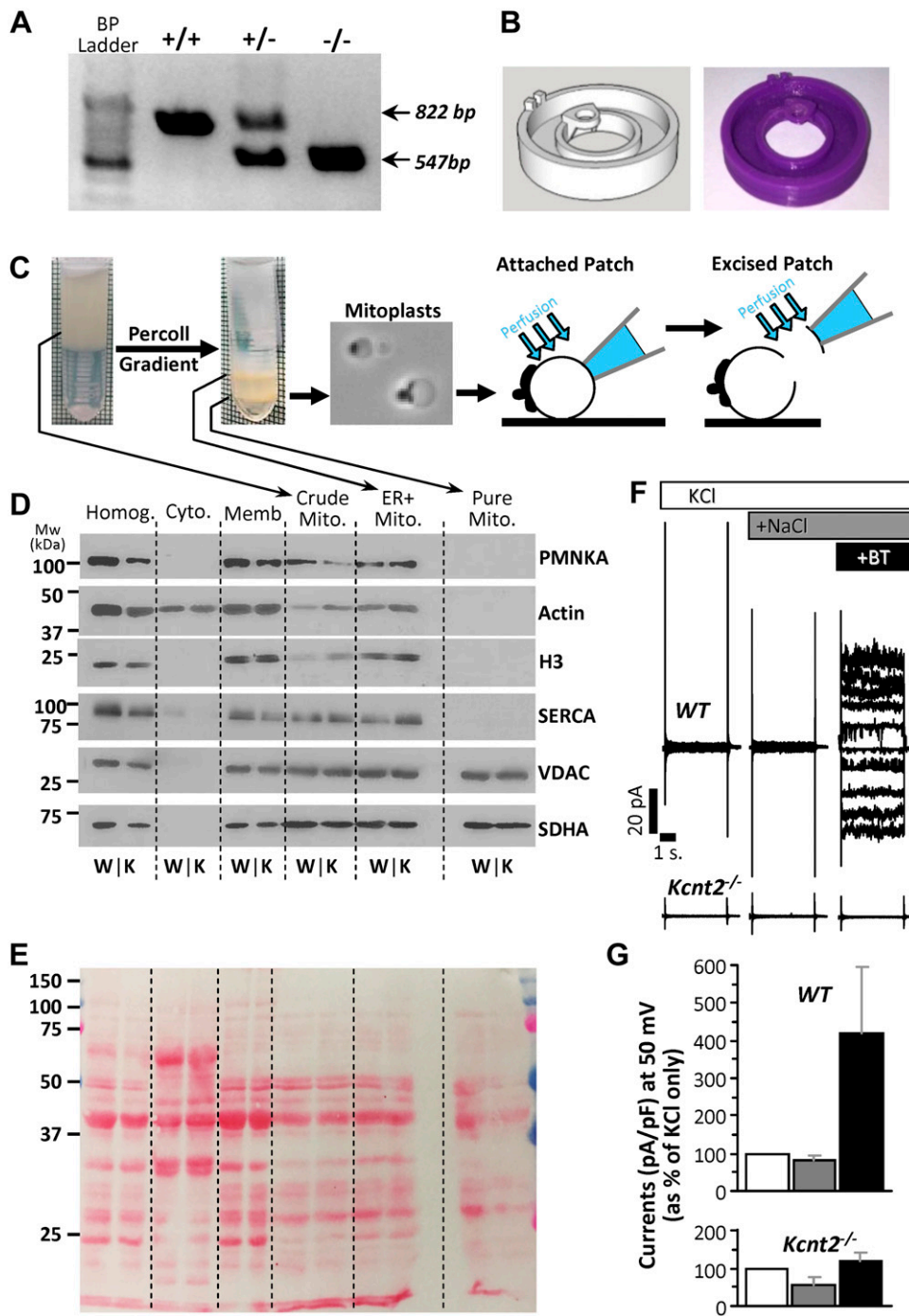


Figure 1. *Kcnt2*^{-/-} mice, mitoplast purification and attached patch clamp. **A**) Example PCR analysis of tail clip genotyping of WT, heterozygous, and *Kcnt2*^{-/-} mice. Amplicon expected for the WT (822 bp) and the knockout (547 bp) alleles. **B**) Custom 3-D-printed micro chamber for patch-clamp analysis of mitoplasts with computer model (left) and final product (right). **C**) Schematic depicting mitochondrial purification, mitoplast preparation, and attached patch and excised patch configuration. **D**) Western blot analysis of proteins from different cellular fractions during mitochondrial purification. Crude Mito, mitochondria-enriched fraction; Cyto, cytosol; ER+Mito, upper band following Percoll; [H3], Histone; Homog, homogenate; Memb, crude membrane; Pure Mito, lower band following Percoll. PMNKA, plasma membrane Na⁺/K⁺-ATPase; SERCA, sarcoplasmic reticulum Ca²⁺-ATPase; VDAC, voltage-dependent anion channel. **E**) Ponceau Red-stained membrane from blot in **D** for the loading control. (An empty lane was inserted between the ER+mit and Pure Mito samples.) **F**) Representative recordings from attached patch clamp of WT and *Kcnt2*^{-/-} mitoplasts, with perfusion of 150 mM KCl (white), after addition of 40 mM NaCl (dark gray), and after addition of 10 μ M BT (black). **G**) Quantitation of traces normalized to pA/pF and shown as percentage increase in current at a holding potential of 50 mV (same color scheme as **F**). Data are means \pm SD ($n = 4-10$ independent mitoplast preparations).

(supplemented with 1.8 mM, CaCl₂ 2.5% fetal bovine serum, and penicillin/streptomycin; 11095-080; Thermo Fisher Scientific, Waltham, MA, USA). Cell viability and yield were determined by Trypan blue and a hemocytometer. Only preparations with >85% viable rod-shaped cells were used for experiments. Cells were seeded at 2000/well on Seahorse XF96 V3-PS plates (Agilent Technologies, Santa Clara, CA, USA) and equilibrated for 1 h. Minimum essential medium was replaced with unbuffered DMEM (pH 7.4) containing various carbon sources (mM: 5 glucose, 0.1 palmitate, 4 glutamine, 5 galactose, 5 lactate, and 1 pyruvate) and either 10 mM 2-deoxyglucose or 20 μ M etomoxir (MilliporeSigma), as detailed in the Results. All conditions with palmitate had 0.1 mM L-carnitine. Oxygen consumption rates (OCRs) were measured with an XF96 extracellular flux analyzer ($n = 5$ WT and 4 *Kcnt2*^{-/-} mice).

Ex vivo heart perfusion

Hearts from male and female mice were perfused in constant flow (4 ml/min.) Langendorff mode as previously described (3). Krebs-Henseleit buffer (KH; in mM: 118 NaCl, 4.7 KCl, 25 NaHCO₃, 1.2 MgSO₄, 1.2 KH₂PO₄, and 2.5 CaCl₂, gassed with 95%/5% O₂/CO₂, 37°C) was supplemented with 5 mM glucose or 0.1 mM bovine serum albumin-conjugated palmitate. Left ventricular pressure was measured *via* a water-filled, transducer-linked left ventricular balloon. Left ventricular and coronary root pressures were monitored and digitally recorded (Dataq, Akron, OH, USA). After equilibration hearts were treated with isoproterenol (100 nM final) for 5 min ($n = 7$ WT and *Kcnt2*^{-/-} mice).

Electron microscopy

Hearts from male and female mice were fixed in 4% paraformaldehyde+2.5% glutaraldehyde in Millonig's phosphate buffer [0.2 M NaH₂PO₄/Na₂HPO₄, and 0.5% NaCl (pH 7.4)]. One millimeter cubes were processed and digitally photographed on a 7650 electron microscope at ×12,000 (Hitachi, Chiyoda, Japan). Analysis of images was performed with ImageJ software (NIH). Mitochondrial areas and densities were placed into 8 or 5 bins, respectively, and the resulting histograms were fitted to a single gaussian. The form factor was calculated as $1/[(4\pi \cdot \text{area})/(\text{perimeter}^2)]$, and the aspect ratio was calculated as major axis/minor axis ($n = 5$; WT and *Kcnt2*^{-/-} mouse hearts, 5 fields of view/heart, and 50 mitochondria/field of view).

Metabolomics

Hearts from male mice were perfused as above in KH buffer supplemented with glucose plus palmitate for 20 min, then freeze clamped with Wollenberger tongs in liquid N₂ and ground to powder. Samples representing ~50% of each heart (50 mg) were shipped to Metabolon (Research Triangle Park, NC, USA) on dry ice, extracted by standard procedures, and analyzed by liquid chromatography–tandem mass spectrometry and gas chromatography MS/MS (Global Metabolomics solution; Metabolon, Inc.) to measure the relative steady-state abundance of metabolites ($n = 7$ /WT and *Kcnt2*^{-/-} group).

Data for each run were median normalized. Overall, 527 metabolites were identified, of which 26 (4.9%) were removed because of insufficient replicates, yielding 7014 theoretical individual data points (501 data points × 7 mice/group × 2 groups). A further 229 outlying data points (>1 SD) were removed, representing 3.3% of the data. Missing values were imputed as weighted medians (25). Metabolomic data were analyzed with Metaboanalyst software (26). In a separate series of experiments, WT and *Kcnt2*^{-/-} hearts were perfused in KH buffer supplemented with fat as the only carbon source, adenine nucleotide levels (ATP, ADP, and AMP) were measured (27), and the energy charge was calculated as $(\text{ATP}+1/2\text{ADP})/(\text{ATP}+\text{ADP}+\text{AMP})$.

Immunoblot analysis

The sample protein was determined by the Folin-Phenol (Lowry) assay. Nonmitochondrial samples were diluted 2 times in Laemmli sample loading buffer and incubated at 95°C for 1 min, whereas mitochondrial samples were diluted 2 times in sample loading buffer containing 5 times the standard concentration of SDS and incubated at 25°C for 30 min. Samples were separated by SDS-PAGE (10% gels) and transferred to nitrocellulose, followed by probing with antibodies as recommended by manufacturer's protocols. Detection employed horseradish-linked secondary antibodies with enhanced chemiluminescence (GE Healthcare, Pittsburgh, PA, USA) ($n = 4$ mice/genotype).

Body composition, fasting glucose response, and electrocardiogram

Body weight from male and female mice was measured once a week, from weaning (3 wk) to 25 wk of age, by weighing non-anesthetized mice placed in a small plastic container on a digital scale. (For both sexes and for each genotype, $n = 14$). Eighty-four-day-old (12 wk) WT and littermate *Kcnt2*^{-/-} male mice were anesthetized as described above, and body fat content was measured with dual-energy X-ray absorptiometry (DEXA) scanning (Lunar PIXImus densitometer; GE Healthcare) ($n = 14$ male WT and *Kcnt2*^{-/-} mice; $n = 8$ female WT and *Kcnt2*^{-/-}

mice). Blood glucose was measured with a True2Go glucose meter with TrueTest glucose strips (Trividia Health, Fort Lauderdale, FL, USA). Mice were unfed overnight in cleaned cages with access to water and cotton bedding (for both sexes and for each genotype, $N = 14$). Alternatively, after anesthesia, electrocardiograms were recorded by 3 needle electrodes and an EKG amplifier (Harvard Apparatus, Cambridge, MA, USA). EKG measurements were averaged for each animal from 10 different segments of the trace, each containing R₁-S₁-T₁-P₂-Q₂-R₂ waves ($n = 4$ WT and 5 *Kcnt2*^{-/-} mice).

Quantitative PCR analysis

mRNA was extracted from heart homogenates with acid phenol/Trizol, according to the Direct-zol RNA MiniPrep Kit R2050 (Zymo Research, Irvine, CA, USA), as described by Toledo-Arena *et al.* (28). cDNAs were prepared with an iScript Kit (170-8891; Bio-Rad, Hercules, CA, USA). qPCR analysis was performed with a PrimePCR regulation of lipid metabolism-PPAR M96 predesigned 96-well panel for use with Sybr Green (10031585; Bio-Rad) ($n = 3$ WT and 3 *Kcnt2*^{-/-} mice).

Replicates and statistics

For samples comparing WT and *Kcnt2*^{-/-}, $n = 1$ is 1 animal (*i.e.*, biologic replicates). Significant differences between the WT and *Kcnt2*^{-/-} groups were determined with 2-way ANOVA with a Bonferroni correction for multiple testing, followed by *post hoc* paired or unpaired Student's *t* tests. A value of $P < 0.05$ indicated significance.

RESULTS

Kcnt2 knockout

Figure 1A shows an example of results of genotyping on WT and *Kcnt2*^{-/-} mice, indicating the expected amplicons. The deletion targets exon 22 of the genomic open reading frame, and results in a complete loss of both mRNA and protein (18), as we have also confirmed in the heart (3).

Cardiac mitochondria contain a K_{Na}1.2 channel

To investigate cardiac mitochondrial K⁺ channels, we performed electrophysiologic studies on Percoll-purified isolated mitochondrial inner membranes (mitoplasts) from hearts of WT or *Kcnt2*^{-/-} mice (Fig. 1C). Mitochondrial enrichment was verified by Western blot analysis for mitochondrial proteins, and purity was confirmed by Western blot analysis for nonmitochondrial membrane proteins (Fig. 1D, E). Mitoplasts were readily identified under light microscopy (Fig. 1C) and high-resistance seals (2–10 GΩ) were formed with the inner membrane opposite the outer membrane cap. In an initial series of experiments using attached mitoplast patch configuration, channel activity in WT was not activated by NaCl alone, but manifested upon further addition of the K_{Na} activator BT (3). No activation by NaCl or BT was seen in *Kcnt2*^{-/-} mitoplasts (Fig. 1F, G). The absence of activation by NaCl alone in WT mitoplasts suggest that the channel's ion-sensing site may be on the matrix side of the inner

membrane and thus was inaccessible to Na^+ from the bath perfusion on this time scale. To investigate such a channel, an excised mitoplast patch was used, affording access to the matrix side of the inner membrane (Fig. 1C).

Channel activity was observed in a high proportion of independent preparations obtained from both WT (85%) and $Kcnt2^{-/-}$ (76%) hearts (Fig. 2A), consistent with previous reports that mitochondria contain numerous K^+ channels (1, 29). In some cases, more than 1 channel was observed in a single preparation, yielding 25 recorded conductances in WT and 42 in $Kcnt2^{-/-}$ preparations. A multiple-level screen was performed to triage recordings containing channels other than $\text{K}_{\text{Na}1.2}$ (Fig. 2B–D). The bath recording solution was sequentially switched from initial (containing 100 μM CaCl_2), to 40 mM LiCl, then

40 mM NaCl, and finally 40 mM NaCl+2.5 μM BT. In each condition, channel activity was monitored at holding potentials from -100 to $+100$ mV.

First, patches exhibiting channel activity in Ca^{2+} alone were discarded, as this is indicative of K_{Ca} channel activity (Fig. 2B, gold). Next, we discarded patches exhibiting activity after the switch to LiCl, as this is indicative of Na^+ -conductance (30) (Fig. 2B, light gray). Next, patches exhibiting channel activity in the presence of activating levels of NaCl (40 mM) and NaCl plus BT (2.5 μM) were considered potential $\text{K}_{\text{Na}1.2}$ candidates (Fig. 2C, blue). Recordings exhibiting channel activity in the presence of Na^+ but not after addition of BT, were also discarded (Fig. 2C, dark gray). Finally, single-channel unitary conductance was compared to the values expected for $\text{K}_{\text{Na}1.2}$

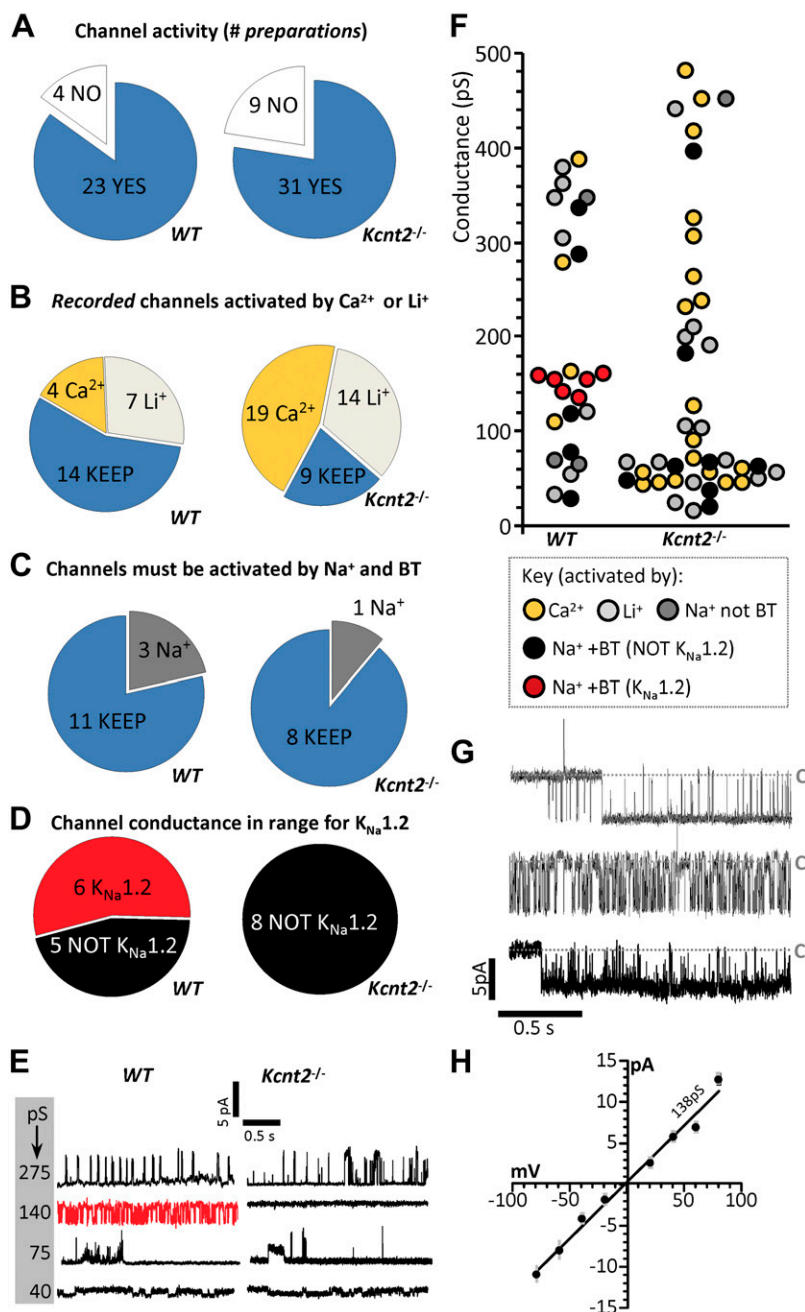


Figure 2. Mitochondria contain a $\text{K}_{\text{Na}1.2}$ channel. **A)** Preparations from WT (left) and $Kcnt2^{-/-}$ (right) mitoplasts, sorted by channels observed (blue) or no channels observed (white). **B)** Exclusion of Ca^{2+} -activated (gold) or Li^+ -activated (light gray) channels. In some preparations, more than 1 channel was observed. **C)** Selection of channels activated by Na^+ and BT, with exclusion of channels activated by Na^+ alone and subsequently blocked by BT (dark gray). **B, C)** Channels carried over to the subsequent screening step are shown in blue. **D)** Selection of channels with peak conductance matching that reported for $\text{K}_{\text{Na}1.2}$ (red). **E)** Example traces of channels observed in WT and $Kcnt2^{-/-}$ preparations with a variety of peak conductances. Red trace indicates a channel assigned as $\text{K}_{\text{Na}1.2}$. **F)** Peak conductance of channels observed from all traces. **B–F)** Color key shown at base of F. Channels with conductance >500 pS are omitted for clarity. **G)** Example of 2 s recordings from 3 $\text{K}_{\text{Na}1.2}$ channels observed in WT mitoplasts (i.e., red points in Fig. 1F) at -40 mV holding potential. Gray dashed line labeled C: closed states. **H)** Channel current vs. voltage plot of peak unitary conductances of all $\text{K}_{\text{Na}1.2}$ channels from WT mitoplast recordings. Average slope conductance was 138 ± 1 pS.

(~140 pS) (15, 30, 31), and those patches exhibiting appropriate conductance were considered to be $K_{Na}1.2$ channels worthy of further analysis (Fig. 2D, red).

Figure 2E shows representative recordings observed in mitoplast patches from WT and *Kcnt2*^{-/-} mice, exhibiting a variety of unitary conductances, with the knockouts having an absence of activity in the conductance range expected for $K_{Na}1.2$. Quantitation of all conductances showed a cluster of 6 channels in WT mitoplasts that passed all screens (Fig. 2F red data points), with no channels of similar conductance observed in *Kcnt2*^{-/-} mitoplasts. The *Kcnt2*^{-/-} recordings contained proportionally more Na⁺- and BT-activated channels than WT in the small-conductance range (Fig. 2F, black symbols in 20–80 pS range, 6/42 *Kcnt2*^{-/-} mice vs. 2/25 WT). A similar observation was made for the mitochondrial BK channel, wherein loss of channels with the expected conductance in a knockout was accompanied by an increase in small-conductance openings (12). Figure 2G shows representative examples of single-channel activity for 3 (of 6) Na⁺- and BT-activated conductances recorded at a holding potential of -40 mV in WT mitoplasts. As reported for $K_{Na}1.2$ (15), these channels showed rapid flickering between open and closed states. The average unitary slope conductance was 138 ± 1 pS (Fig. 2H, peak conductance graph for all 6 channels). In our buffer conditions, reversal potential for channels conducting Na⁺ or Cl⁻ was predicted to be -23 or -8 mV, respectively. K⁺ was the only other ion present and the channel current crossed 0 at -2 mV, and this finding indicates that K⁺ was the predominant conducting ion. The data in Fig. 2 demonstrate that WT cardiac mitochondria contained a K⁺ channel with the ion selectivity, ion sensitivity, pharmacology, and conductance properties of $K_{Na}1.2$ that are absent in mitochondria from *Kcnt2*^{-/-} mice.

Electrophysiological characterization of mitochondrial $K_{Na}1.2$

Single-channel characteristics are useful for classifying channels. Of the 2 K_{Na} channels; $K_{Na}1.1$ (*Kcnt1/Slack/SLO2.2*) and $K_{Na}1.2$ (*Kcnt2/Slick/SLO2.1*), $K_{Na}1.1$ has been described in more detail at the single-channel level. Where possible, we compared the characteristics of the channels measured in this study to those published for $K_{Na}1.2$ (15, 30, 31). If this was not possible, a comparison to $K_{Na}1.1$ was included, given that both K_{Na} channels share similar characteristics, and it is known that $K_{Na}1.1$ is not present in the heart (3, 18).

A detailed single-channel analyses of all 6 assigned $K_{Na}1.2$ patches was not possible because of the presence of 2 or more identical channels within some patches (Fig. 3A), which is in agreement with previous reports that $K_{Na}1.2$ channels cluster in neuronal plasma membranes (32). Examination of all suitable WT recordings (representative example, Fig. 3B) revealed a higher open probability at negative potentials (Fig. 3C). In addition, as previously reported for $K_{Na}1.2$ (15, 33), numerous distinct subconductances were apparent between 35 and 140 pS (Fig. 3D). This behavior is a characteristic of $K_{Na}1.1$ channels (34, 35),

and although it has been observed in $K_{Na}1.2$ mutants (33), this is the first observation of such in WT $K_{Na}1.2$ channels in endogenous membranes. The average slope conductance when considering all subconductances was 75 pS (Fig. 3E), which agreed well with the average chord conductance of 74.8 ± 6.8 pS (assuming reversal potential of 0 mV). These data indicate that smaller subconductance states predominate in the active channel current.

Open and closed channel dwell times were also calculated from continuous recordings at -40 mV (representative 45 s example, Fig. 3F). The frequency of channel open and closed dwell times was fitted to the sum of multiple simple exponentials, constituting 94.6% of the total area under the curve, and subsequent log-binned histograms revealed peaks representing 3 closed times and 2 open times (Fig. 3G). The longest closed time ($\tau_3 = 262$ ms) represents periods of channel closure between bursts of activity, which is characteristic of $K_{Na}1.2$ (15).

$K_{Na}1.2$ channel activation uncouples cardiomyocyte oxidative phosphorylation

We next sought to determine the impact of cardiac $K_{Na}1.2$ channel activity on cardiomyocyte bioenergetics. Using Seahorse XF analysis, we measured OCRs of cardiomyocytes from WT and *Kcnt2*^{-/-} mice. Cells from both genotypes had similar viability and rod-shaped morphology (Fig. 4A). The K_{Na} opener BT (2.5 μ M) significantly stimulated OCR in oligomycin-treated cardiomyocytes from WT mice, but not those from *Kcnt2*^{-/-} mice (WT, 370 ± 48 maximum OCR; *Kcnt2*^{-/-}, 154 ± 32 maximum OCR) (Fig. 4B). The marginal but persistent effect of BT in *Kcnt2*^{-/-} cells is consistent with the observation of small conductances activated by Na⁺ and BT in *Kcnt2*^{-/-} mitoplast patches (Fig. 2F).

In the mitochondrial K⁺ cycle (36), K⁺ entry into the organelle activates a mitochondrial K⁺/H⁺ exchanger, such that mitochondrial K⁺ channel activity can uncouple oxidative phosphorylation. The much larger BT-induced respiratory stimulation in WT vs. *Kcnt2*^{-/-} cardiomyocytes is most likely related to mitochondrial uncoupling. As an additional control, the *bona fide* mitochondrial uncoupler carbonyl cyanide-*p*-trifluoromethoxyphenylhydrazone (FCCP) elicited similar maximum respiration rates in cardiomyocytes from both genotypes (WT, 387 ± 15 maximum OCR; *Kcnt2*^{-/-}, 364.2 ± 53 maximum OCR), rendering it unlikely that the differential effect of BT in WT vs. *Kcnt2*^{-/-} cells is related to an underlying difference in overall bioenergetic capacity. Consistent with this result, Western blot analysis for several mitochondrial marker enzymes [succinate dehydrogenase complex, subunit A (SDHA), isocitrate dehydrogenase, cyclophilin-D, and electron transfer flavoprotein, subunit α] suggested no difference in mitochondrial mass or content between WT and *Kcnt2*^{-/-} hearts (Fig. 4C).

Loss of $K_{Na}1.2$ mildly impacts cardiac mitochondrial ultrastructure

An important function of the mitochondrial K⁺ cycle is the regulation of organelle volume (37, 38), and $K_{Na}1.2$ activity

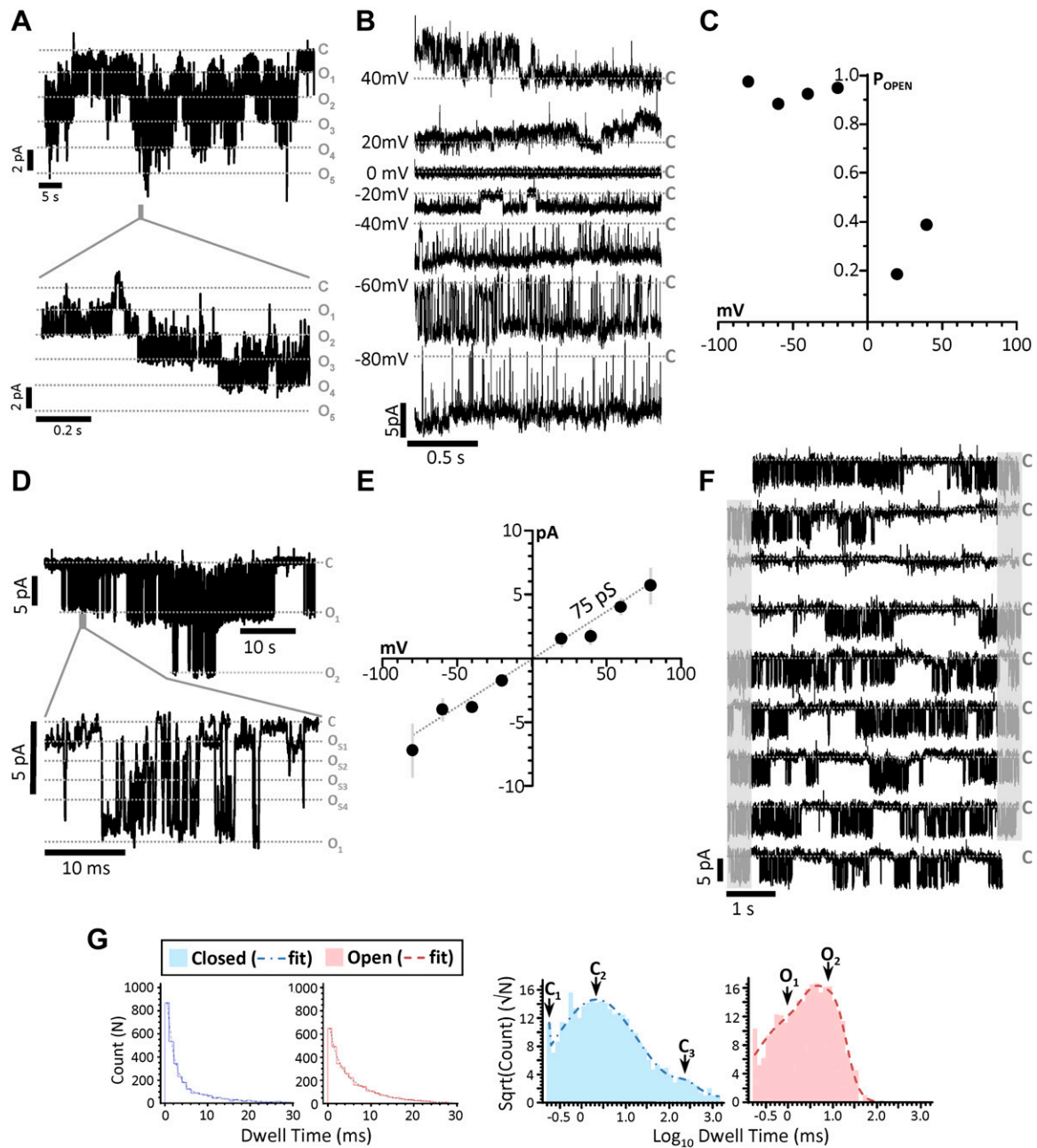
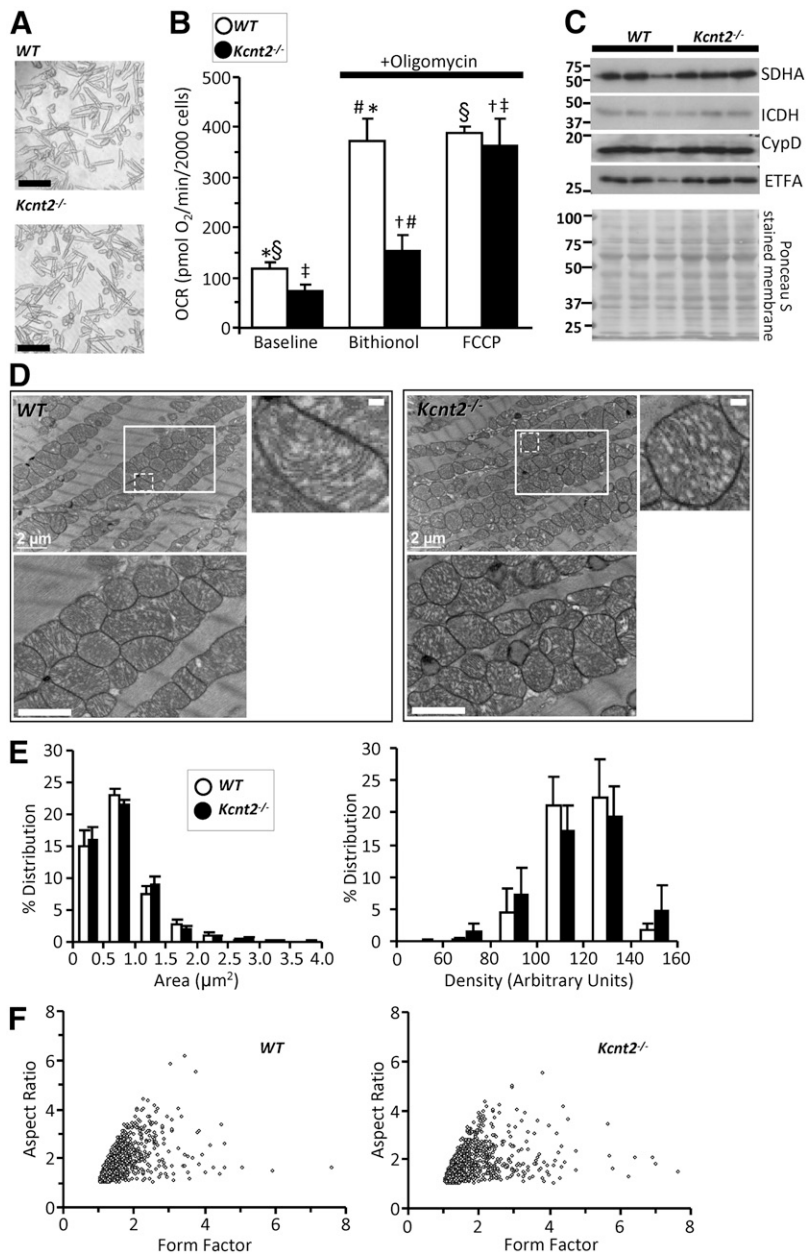


Figure 3. Single-channel characteristics of mitochondrial $K_{Na}1.2$. *A*) Compressed traces from the recording of a patch containing 5 mitochondrial $K_{Na}1.2$ channels (holding potential, -20 mV), and a time-expanded trace for the region highlighted by the gray bar in the trace above. Gray dashed lines: closed (C) and multiple open (O) states. *B*) Traces from a single $K_{Na}1.2$ channel at holding potentials of 40 to -80 mV. *C*) Channel open probability plot from the channel shown in *B*. *D*) Representative trace of a recording with 2 channels on a compressed time scale (holding potential -40 mV) and a time-expanded trace for the region highlighted by the gray bar in the trace above, showing multiple subconductance states within the channel peak conductance (e.g., O_{S1}). *E*) Current-voltage relationship of all 6 mito- $K_{Na}1.2$ channels showing average current at each holding potential. The decreased slope conductance (compared to Fig. 2H showing peak unitary conductance) indicates that subconductances averaging 75 pS dominated the average current during the recordings. *F*) Continuous trace (45 s) of a single channel. Gray shading: portions of each trace (right) that are repeated (left) on the next line. Gray dashed lines labeled C: closed states. *G*) Log binned channel closed and open dwell-time peaks and frequency of closed dwell times plotted against their duration. Table inset shows calculated area and time constants (τ).

is known to be sensitive to osmolarity (39, 40). Thus, we hypothesized that mitochondria from $Kcnt2^{-/-}$ may exhibit ultrastructural changes. Electron microscopic analysis of hearts from WT and $Kcnt2^{-/-}$ mice (Fig. 4D-F) revealed that mitochondria had similar areas (WT, $0.9 \pm 0.30 \mu\text{m}^2$; $Kcnt2^{-/-}$, $0.89 \pm 0.43 \mu\text{m}^2$; mean \pm SD; $n = 5$)

and matrix density (WT, 134 ± 17 ; $Kcnt2^{-/-}$, 135 ± 24 ; mean \pm SD; $n = 5$). The distribution of these parameters (Fig. 4E) suggested a small shift toward increased area and density in $Kcnt2^{-/-}$ vs. WT, but it was not statistically significant. In addition, no difference in either form factor or aspect ratio was observed between the genotypes

Figure 4. *Kcnt2*^{-/-} Cardiomyocyte bioenergetics and mitochondrial ultrastructure. **A)** Representative images of isolated cardiomyocytes from WT and *Kcnt2*^{-/-} hearts. Scale bars, 100 μ m. **B)** OCR of isolated cardiomyocytes measured with addition of oligomycin (1 μ g/ml) and either 2.5 μ M BT (K_{Na} opener) or 500 nM FCCP (mitochondrial uncoupler). Statistics were measured using 2-way ANOVA with Bonferroni correction and *post hoc t* test. Bars with the same symbol are significantly different from each other ($n = 4-5$). Data are means \pm SEM. $P < 0.05$. **C)** Western blots from WT and *Kcnt2*^{-/-} heart homogenates showing levels of mitochondrial proteins (SDHA, isocitrate dehydrogenase, cyclophilin D, and electron transfer flavoprotein subunit α) and Ponceau stain loading control. **D)** Representative transmission electron microscopic images of fixed heart slices. Bottom left panels: insets boxes at higher magnification. Scale bar, 1 μ m. Top right panels: increased magnification of single mitochondria from WT and *Kcnt2*^{-/-} mice with mitochondrial ultrastructure visible (*i.e.*, cristae folds, outer and inner membrane contacts). Scale bar, 200 nm. **E)** Binned histogram of mitochondrial area or mitochondrial density, obtained from image analysis ($n = 5$). Data are means \pm SD for each bin. **F)** Form-factor/aspect-ratio scatterplot. **E, F)** Data obtained from 1250 mitochondria, 25 fields of view, and 5 WT or *Kcnt2*^{-/-} hearts.



(Fig. 4F), indicating that $K_{Na}1.2$ deficiency does not alter mitochondrial fission or fusion (41, 42). Together, the data in Fig. 4 suggest that, although activation of $K_{Na}1.2$ can uncouple respiration, loss of the channel does not impact cardiac mitochondrial structure or content.

$K_{Na}1.2$ is necessary for cardiac respiratory reserve capacity when oxidizing fat

In an effort to further understand the bioenergetic effects of $K_{Na}1.2$ deficiency, we compared metabolic substrate preferences in cardiomyocytes isolated from WT and *Kcnt2*^{-/-} mice. Myocytes were incubated with 1) glucose alone (with etomoxir to inhibit fatty acid β -oxidation), 2) palmitate alone (with 2-deoxyglucose to inhibit glycolysis), or 3) glucose+palmitate. The response to uncoupling by FCCP (500 nM) was used to determine respiratory reserve (RR) capacity under each substrate condition (Fig. 5A–C).

Cardiomyocytes from WT and *Kcnt2*^{-/-} cells exhibited a similar baseline OCR under all substrate conditions (Fig. 5B). In WT cells, a robust uncoupling response to FCCP was seen under all conditions, and notably, the uncoupling response with palmitate alone (3.3-fold) was equal to that seen when both substrates were present (3.3-fold). However, in *Kcnt2*^{-/-} cells, the uncoupling response with palmitate alone (2.4-fold) was significantly blunted compared with that seen when both substrates were present (4.3-fold) (comparison between blue and purple bars in left and right panels of Fig. 5B). The additional OCR induced over baseline by FCCP was used to calculate RR capacity. Figure 5C shows that the RR of WT and *Kcnt2*^{-/-} cells was similar in the glucose alone and the glucose+palmitate conditions. However, with palmitate alone, *Kcnt2*^{-/-} cells exhibited a significant RR deficit relative to WT. No such RR deficit was observed in myocytes from *Kcnt2*^{-/-} mice respiring on lactate, glutamine, galactose, or pyruvate

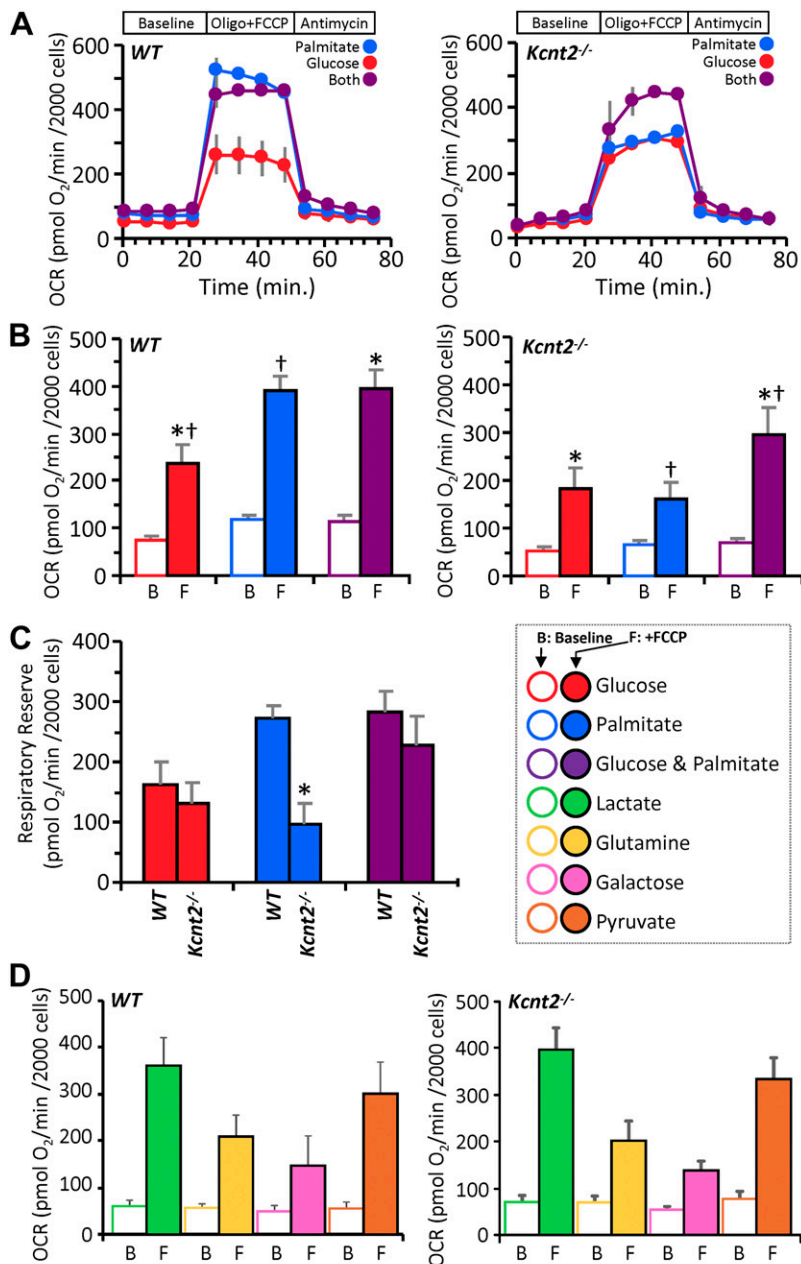


Figure 5. KNa1.2 loss impacts cardiac metabolic substrate choice under stress. *A*) Representative OCR traces of isolated WT or *Kcnt2*^{-/-} cardiomyocytes, incubated in the presence of different metabolic substrates. Data from a single XF plate are shown (mean ± SD of 12 wells/substrate or genotype). Timeline above traces shows the OCR was measured at baseline, then with the addition of the ATP synthase inhibitor oligomycin (1 μg/ml) plus the mitochondrial uncoupler FCCP (500 nM), and finally with the mitochondrial complex III inhibitor antimycin A (5 μM). *B*) Group OCR averages of baseline (B) and FCCP-uncoupled (F) cardiomyocytes under substrate conditions as defined above. Statistics were measured using 2-way ANOVA with Bonferroni correction and *post hoc* Student's *t* test. Data are mean ± SEM, for *n* = 4 *Kcnt2*^{-/-} or 5 WT, independent cardiomyocyte preparations. Bars with the same symbol are significantly different from one another. *P* < 0.05. *C*) RR capacity calculated from the data in *B* (*i.e.*, uncoupled minus baseline OCR). Mean ± SEM (*n* = 4–5). **P* < 0.05 between genotypes. Color key for metabolic substrates used in all panels is shown to the right of *C*. *D*) OCR of WT and *Kcnt2*^{-/-} cardiomyocytes metabolizing different substrates. Empty bars, baseline (B); filled bars, FCCP uncoupled (F). Data are means ± SEM from 4 to 5 independent cardiomyocyte preparations.

(Fig. 5D), indicating that the *Kcnt2*^{-/-} RR deficit is specific to fat oxidation.

To test the physiological relevance of this RR deficit, the ability of perfused hearts to respond to increased metabolic demand was tested. Hearts from WT and *Kcnt2*^{-/-} mice were perfused with palmitate as the sole carbon source, whereas stimulating workload by addition of the β-adrenergic agonist isoproterenol (100 nM). Hearts from *Kcnt2*^{-/-} mice showed a significantly reduced functional response to isoproterenol, relative to WT (WT, 213 ± 20% increase in rate × pressure product (RPP), *vs.* *Kcnt2*^{-/-} 159 ± 13%; mean ± SEM, *n* = 7) (Fig. 6A). When RPP was broken into its component parameters, a greater difference in the effect of isoproterenol was observed on left-ventricular developed pressure than on heart rate (peak/baseline left-ventricular developed pressure: WT, 135 ± 9% *vs.* *Kcnt2*^{-/-} 114 ± 4%; peak/baseline heart rate: WT, 162 ± 22% *vs.*

Kcnt2^{-/-} 140 ± 9%). However, consistent with the isolated cardiomyocyte OCR data (Fig. 5C), no difference in the isoproterenol-induced functional response was observed when the perfusion buffer was supplemented with glucose and palmitate (Fig. 6A, inset). Together, these data suggest that loss of K_{Na}1.2 results in an impaired ability to respond to increased metabolic demand when oxidizing only fat. Consistent with previous reports (3, 18) no EKG differences were observed in *Kcnt2*^{-/-} mice (Fig. 6B), suggesting that loss of K_{Na}1.2 *per se* does not affect cardiac contractile function.

Whole-animal metabolic differences in *Kcnt2*^{-/-} mice

Because the heart is a major fat-burning organ, we hypothesized that the fat-specific RR capacity deficit in

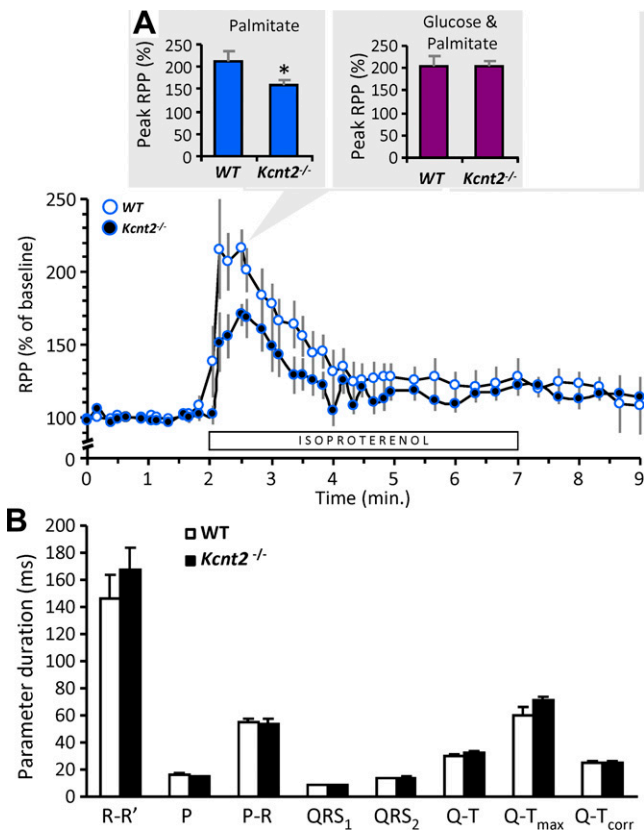


Figure 6. Loss of KNa1.2 impacts whole heart substrate choice under stress. *A*) Cardiac function data (heart rate \times pressure product, RPP) for isolated perfused hearts from WT or *Kcnt2*^{-/-} mice, perfused with Krebs-Henseleit (KH) buffer containing palmitate as the sole metabolic substrate. Bar below the traces indicates duration of 100 nM isoproterenol infusion. Graph shows RPP as a percentage of the average baseline value for 1 min. before isoproterenol infusion. Inset: comparison of the peak response to isoproterenol under this substrate condition (palmitate only, blue). Adjacent inset (right): the peak response to isoproterenol from a separate series of perfusions in which the KH buffer contained both palmitate and glucose as substrates (purple). Data are means \pm SEM ($n = 7$). $*P < 0.05$ between genotypes. *B*) EKG parameters obtained *in vivo* from tribromoethanol-anesthetized WT and *Kcnt2*^{-/-} mice. R-R', distance between R waves of each beat (*i.e.*, 1/HR); P, P-wave duration; P-R, interval between P and R waves; QRS₁ & QRS₂, diameter of QRS complex (different calculation algorithms); Q-T, interval between Q and peak of T wave; Q-T_{max}, interval between Q and end of T wave; Q-T_{corr}, QT interval corrected for heart rate. Data are mean \pm SD ($n = 4-5$ animals).

Kcnt2^{-/-} would be accompanied by metabolic perturbations at the whole-animal level. No significant differences in weight gain were observed between WT and *Kcnt2*^{-/-} mice over 25 wk (Fig. 7A). The percentage of body fat content determined by DEXA analysis (Fig. 7B) revealed a small difference in average fat content between genotypes (WT, 12.6 \pm 3% *vs.* *Kcnt2*^{-/-} 14.6 \pm 4%), but that was statistically significant between paired littermates with (Fig. 7C). In addition, whereas WT mice showed an expected drop in blood glucose after food was withheld overnight (15 h), no such decrease was seen in *Kcnt2*^{-/-} mice (Fig. 7D), suggesting elevated gluconeogenesis in response to unfed state in *Kcnt2*^{-/-}, which is consistent

with a potential increased reliance on glucose oxidation as a compensatory response to the fat-specific RR defect under stress conditions.

Metabolomic and expression profiling of *Kcnt2*^{-/-} hearts

To investigate the molecular underpinnings of the fat-specific RR defect in *Kcnt2*^{-/-} hearts, expression of metabolic regulatory genes was measured using a pre-designed qPCR array (Fig. 8A and Table 1). No differences were observed between WT and *Kcnt2*^{-/-} hearts, suggesting that the fat-specific RR defect is not related to a remodeling of metabolism at an expression level. Separately, a small but nonsignificant decrease in energy charge (ATP+1/2ADP)/(ATP+ADP+AMP) was observed in *Kcnt2*^{-/-} mice (WT, 0.87 \pm 0.05 *vs.* *Kcnt2*^{-/-}, 0.77 \pm 0.03; mean \pm SEM, $n = 5-6$), suggesting that energy-sensing metabolic regulators such as AMPK may be

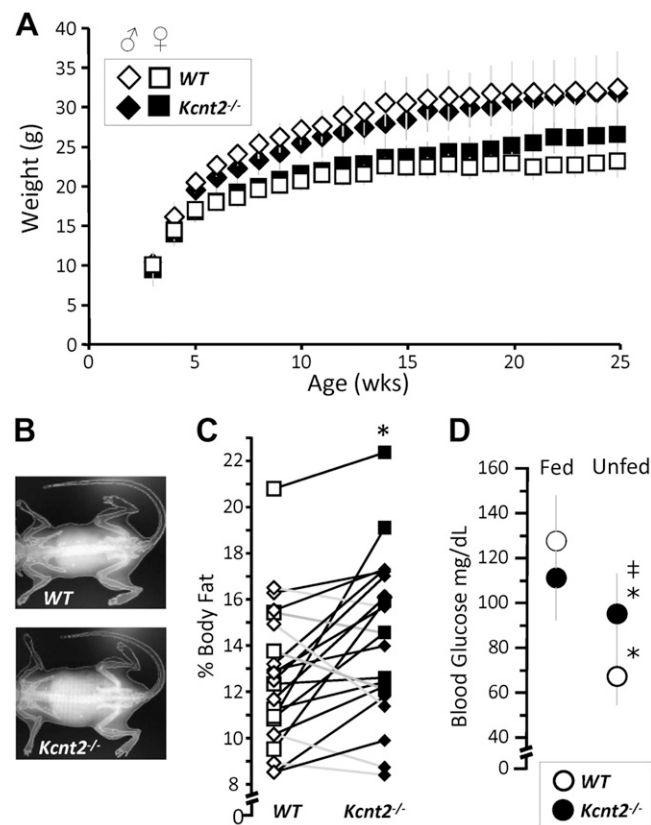


Figure 7. Loss of KNa1.2 impacts whole body metabolic phenotype. *A*) Body weights of WT and *Kcnt2*^{-/-} male (diamond) and female (square) mice from weaning (3 wk) to 25 wk of age. Data are mean \pm SD ($n = 12$). *B*) Representative DEXA images from WT and *Kcnt2*^{-/-} mice. *C*) Percentage of body fat measured by DEXA scan of WT (white symbols) and *Kcnt2*^{-/-} (black symbols) littermates (pairs are indicated by connected data points) ($n = 14$). WT, 8 *Kcnt*^{-/-}. $*P < 0.05$ between genotypes by paired Student's *t* test. *D*) Left: blood glucose levels measured in WT and *Kcnt2*^{-/-} mice at baseline (5 PM, fed) and following a 15-h withdrawal from food (8 AM, unfed). Data are mean \pm SD ($n = 12$). $*P < 0.05$ between fed and unfed states within a genotype, $^{\ddagger}P < 0.05$ between genotypes.

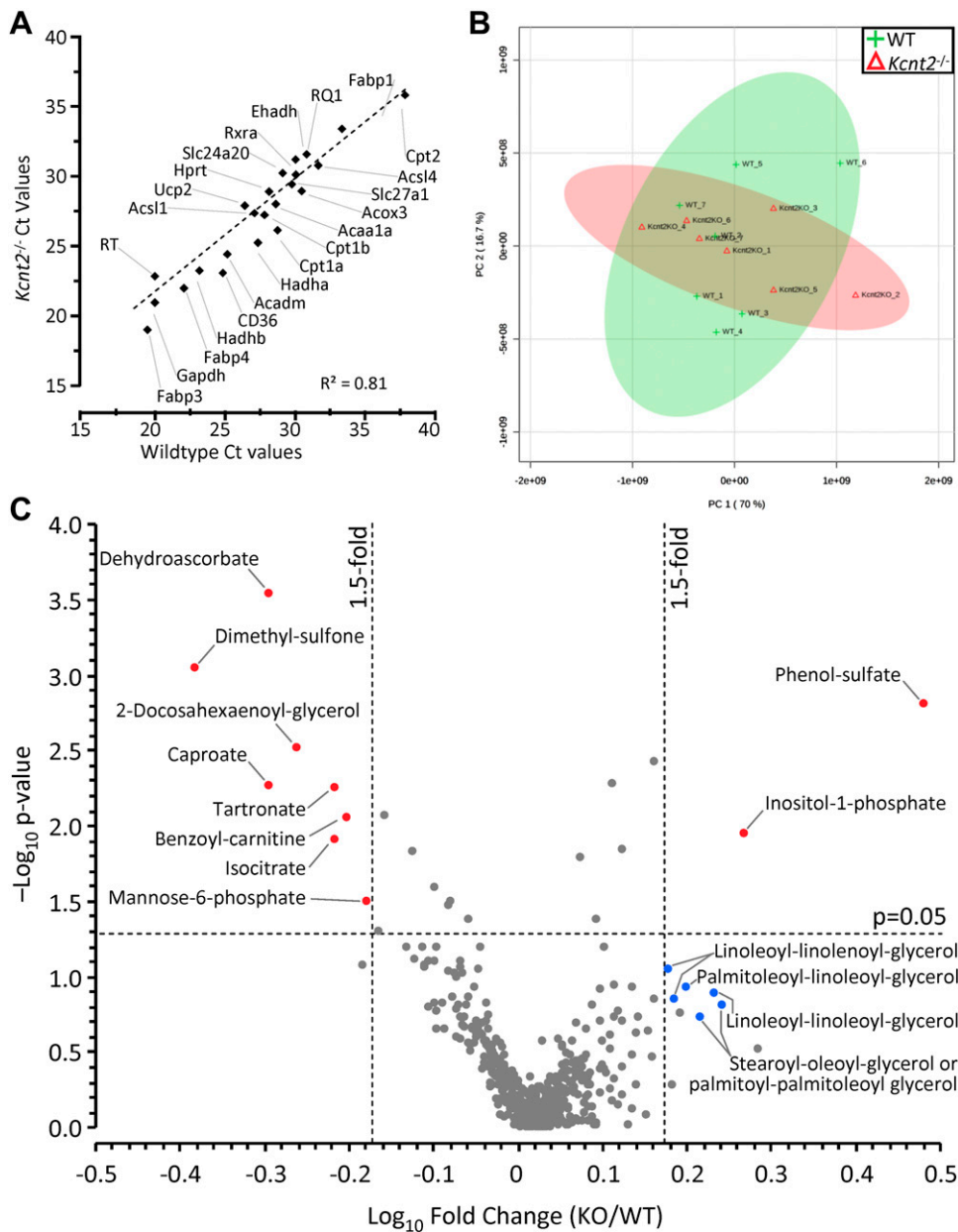


Figure 8. *Kcnt2*^{-/-} cardiac expression profiling and metabolomics. **A)** qPCR *C_t* values for 27 metabolically important genes (Table 1) in WT and *Kcnt2*^{-/-} hearts (*n* = 3 independent RNA preparations/genotype). Data are mean, errors are omitted for clarity. **B)** WT and *Kcnt2*^{-/-} hearts were perfused with KH buffer containing palmitate+glucose and freeze clamped for metabolomic analysis by liquid chromatography-MS/MS. Graph shows principle component analysis of 501 cardiac metabolites. The first and second principal components contributed 86.7% of the overall metabolic character. Shaded ovals overlaying the graph indicate 95% confidence intervals for WT (lime) and *Kcnt2*^{-/-} (salmon pink) samples. **C)** Volcano plot of the metabolic profile of *Kcnt2*^{-/-} vs. WT hearts. Dashed lines: *P* = 0.05 cut off (y axis) and 1.5-fold change cut off (x axis). Each point represents a single metabolite, and each point represents means (*n* = 7 mice). Errors are omitted for clarity. Red: metabolites meeting fold-change and *P*-value criteria; blue: additional metabolites discussed in the text. Diamonds: males; circles: data from both sexes combined.

altered. However, Western blot analysis revealed no difference in AMPK phosphorylation between WT and *Kcnt2*^{-/-} hearts (data not shown). Together with data in Figs. 4 and 5, these findings suggest that *K_{Na}1.2* deficiency does not induce large-scale remodeling of cardiac mitochondrial metabolism. Rather, *K_{Na}1.2* loss specifically affects cardiac fat oxidation only under conditions of high-energy demand such as uncoupling or β -adrenergic stimulation.

Finally, to understand the effects of *K_{Na}1.2* deficiency on cardiac metabolism at a systems level, an unbiased metabolomics analysis was performed. Principal component analysis showed no significant difference in the fundamental character of metabolism between WT and *Kcnt2*^{-/-} hearts at baseline (Fig. 8B). A volcano plot for all 501 metabolites measured revealed only 10 were significantly altered (>1.5-fold vs. WT; *P* < 0.05) (Fig. 8C). Of these metabolites, notable changes were an increase in phenol-sulfate and decrease

in dimethyl-sulfone, potentially indicating perturbations in aryl-sulfotransferase activity and sulfur metabolism. Dehydroascorbate was significantly lower in *Kcnt2*^{-/-} hearts, potentially indicating lower oxidative load. In addition, inositol-1-phosphate was significantly elevated, and a cluster of diacylglycerol metabolites was also elevated (although no individual diacylglycerol approached significance), suggesting enhanced PLC activity in *Kcnt2*^{-/-}. Overall, the comparatively minor nature of metabolomic perturbations in *Kcnt2*^{-/-} hearts at baseline is consistent with the notion that the impact of *K_{Na}1.2* loss is limited to fat oxidation under conditions of high energy demand.

DISCUSSION

A plethora of studies have identified mitochondrial *K⁺* channels at the phenomenological level [reviewed in refs.

TABLE 1. Gene names and symbols for genes targeted by BioRad PrimePCR qPCR assay kit

Gene name	Gene symbol
Acetyl-coenzyme A acyltransferase 1A	<i>Acaa1a</i>
Carnitine palmitoyltransferase 1a, liver	<i>Cpt1a</i>
Hydroxyacyl-coenzyme A dehydrogenase/3-ketoacyl-coenzyme A thiolase/enoyl-coenzyme A hydratase (trifunctional protein), α subunit	<i>Hadha</i>
Acyl-coenzyme A dehydrogenase, medium chain	<i>Acadm</i>
Carnitine palmitoyltransferase 1b, muscle	<i>Cpt1b</i>
Hydroxyacyl-coenzyme A dehydrogenase/3-ketoacyl-coenzyme A thiolase/enoyl-coenzyme A hydratase (trifunctional protein), β subunit	<i>Hadhb</i>
Glyceraldehyde-3-phosphate dehydrogenase	<i>Gapdh</i>
Acyl-Coenzyme A oxidase 3, pristanoyl	<i>Acox3</i>
Carnitine palmitoyltransferase 2	<i>Cpt2</i>
Hypoxanthine guanine phosphoribosyl transferase	<i>Hprt</i>
Acyl-CoA synthetase long-chain family member 1	<i>Acs1l</i>
Enoyl-Coenzyme A, hydratase/3-hydroxyacyl Coenzyme A dehydrogenase	<i>Ehhadh</i>
Retinoid X receptor α	<i>Rxra</i>
PrimePCR DNA contamination control assay	<i>gDNA</i>
Fatty acid binding protein 1, liver	<i>Fabp1</i>
Solute carrier family 25 (mitochondrial carnitine/acylcarnitine translocase), member 20	<i>Slc25a20</i>
PrimePCR positive control assay	<i>PCR</i>
Acyl-CoA synthetase long-chain family member 4	<i>Acs14</i>
Solute carrier family 27 (fatty acid transporter), member 1	<i>Slc27a1</i>
PrimePCR RNA quality assay	<i>RQ1</i>
Fatty acid binding protein 3, muscle and heart	<i>Fabp3</i>
CD36 antigen	<i>Cd36</i>
Fatty acid binding protein 4, adipocyte	<i>Fabp4</i>
Uncoupling protein 2 (mitochondrial, proton carrier)	<i>Ucp2</i>
PrimePCR reverse transcription control assay	<i>RT</i>

Genes are those shown in Fig. 8A.

(1, 43)], and several studies have linked these channels mechanistically to protection against IR injury (1, 44–46). However, surprisingly few examples exist of *bona fide* mitochondrial K^+ channels that are: 1) identified at the molecular (genetic) level, 2) characterized with robust electrophysiology, and 3) linked to any specific mitochondrial channel function phenotype [examples include $K_{Ca}1.1$ (11, 12), K_{ATP} (10), and SK3 (47)]. Although the phenomenon of a cell surface K_{Na} channel was first characterized in hearts 30 yr ago, the field of K_{Na} research rapidly transitioned to study of these channels in brain (19). As such, very little is known about the role of K_{Na} in cardiomyocytes, including potential subcellular localization. In patch-clamp studies of isolated cardiac mitochondrial inner membranes, we recorded a K^+ channel matching the known characteristics of $K_{Na}1.2$ (ion sensitivity, ion selectivity, pharmacology, and conductance) in mitoplasts from WT mice, that was absent in those from *Kcnt2*^{-/-} mice (Figs. 1–3). This is the first report of a K_{Na} channel in mitochondria.

Cardiac mitochondria are reported to contain several cation and anion channels (48, 49), and mitoplast recordings were subjected to a rigorous screening process to ensure that conductances assigned as $K_{Na}1.2$ did not originate from other channels. Bath:pipette ratios of the major ion components (K^+ , Na^+ , and Cl^-) enabled reversal potentials to be differentiated. The Na^+ surrogate Li^+ was used to screen out any Na^+ -activated currents that were in fact related to Na^+ conductance. In addition, any conductances activated by Ca^{2+} were dismissed, to ensure

patched membranes were free of K_{Ca} channels. Inner membrane anion channels and intracellular chloride channel variety exhibit conductances (~ 100 pS: inner membrane anion channels, ~ 8 pS: chloride channel-4) sufficiently distinct from $K_{Na}1.2$ that, in combination with the observed reversal potential, we are confident do not contribute to assigned K_{Na} conductances. Similarly, $mitoK_{ATP}$ channels (~ 10 pS) would not be mistaken for $K_{Na}1.2$. Finally, $K_{Na}1.2$ activation is significantly enhanced by Cl^- in the presence of activating Na^+ , hence Cl^- salts were used to maximize the probability of detecting these channels (15). Of 25 recordings in WT mitoplasts, this strategy yielded 6 channels, a 24% success rate. Application of this rate to the 42 recordings in *Kcnt2*^{-/-} mitoplasts predicts 10 such channels, but we observed none.

Several known electrophysiological characteristics of $K_{Na}1.2$ channels were also observed in our assigned $K_{Na}1.2$ mitoplast recordings, including: 1) multiple subconductance states (Fig. 3D) (15, 35), 2) rapid flickering between open and closed states (Fig. 2G) (15), 3) burst operation with prolonged closed times between bursts (Fig. 3F, G) (15, 50), and 4) multiple channels within the same patch is consistent with the hypothesis that these channels form clusters in membranes, although could also arise from the random presence of 2 or more channels in a single patch (Fig. 3A) (35). In combination with the absence of such conductances in *Kcnt2*^{-/-} mitoplasts, these characteristics strengthen the conclusion that the genetic origin of the channels herein designated $mitoK_{Na}1.2$, is the *Kcnt2* gene product. Whole-mitoplast attached patch experiments (Fig. 1E) suggest that

the orientation of the channel in the mitochondrial inner membrane is the same as that reported for plasma membrane $K_{Na}1.2$ —namely, with the C-terminal Na^+ -sensing site on the inside of the membrane (15, 51).

Patches from WT and $Kcnt2^{-/-}$ recordings contained channels with a similar overall range of conductances. However, the distribution of these conductances between genotypes was shifted. In particular, channels with unitary conductances in the range of 20–80 pS were more frequently observed in $Kcnt2^{-/-}$ (Fig. 2F). A similar observation was recently made with a cardiac-specific knockout of the mito-BK channel (12), raising the intriguing possibility that loss of 1 mitochondrial K^+ channel may lead to compensatory up-regulation of other channels, to maintain K^+ homeostasis. Given the importance of the mitochondrial K^+ cycle for the regulation of organelle volume (36), such compensatory K^+ fluxes may account for the persistence of a small but nonsignificant respiratory uncoupling effect of BT in $Kcnt2^{-/-}$ cardiomyocytes (Fig. 4B), as well as the relatively minor effect of $K_{Na}1.2$ loss on mitochondrial ultrastructure (Fig. 4D–F). An alternative to compensatory expression between different mitochondrial K^+ channels, is the possibility they may form heteromers. Individual $K_{Na}1.1$ ($Kcnt1$) subunits can combine with $K_{Ca}1.1$ [potassium calcium-activated channel subfamily M $\alpha 1$ gene ($Kcnma1$)] subunits to form functional heterotetramers of intermediate conductance and activation properties (14). Heterotetramers of $K_{Na}1.1$ with $K_{Na}1.2$ have also been demonstrated (35). However, the existence of $K_{Ca}1.1/K_{Na}1.2$ heterotetramers has not been reported.

A key aspect of these studies was the discovery that loss of cardiac $K_{Na}1.2$ results in a unique metabolic phenotype—namely, a specific defect in cardiac fat oxidation only under conditions of high energy demand. An important caveat is that we cannot definitively rule out the possibility that the metabolic phenotype of $Kcnt2^{-/-}$ is related to loss of the channel at the plasma membrane. However, this is true of all proteins that are expressed at both the plasma membrane and the mitochondria. Despite the development of anti- K_{Na} antibodies, fluorescent tags, and K_{Na} channel-knockout animals, the channel's existence at the cardiac plasma membrane has not been confirmed using any of these methods during the intervening time period. In addition, the $Kcnt2^{-/-}$ mouse is a global knockout, and it is possible that $K_{Na}1.2$ loss from other cell types contributes to the phenotypes observed in our study. $K_{Na}1.2$ is broadly expressed in most regions of the brain and CNS, with similar expression levels in cardiac tissues and ovaries, although its relative expression is an order of magnitude lower in all other tissues measured (18). Currently, there are no reports exploring the function of K_{Na} channels in cell types, other than neurons and cardiac myocytes. Because the metabolic phenotype we observed was acutely activated in isolated hearts and in cardiac myocytes, the most likely origin is cardiac $K_{Na}1.2$. Coupled with definitive data herein demonstrating existence of $K_{Na}1.2$ in cardiac mitochondria, and previous reports of a BT-activated mitochondrial K^+ channel that is absent in isolated mitochondria from both *C. elegans* $Slo2^{-/-}$ (52) and mouse $Kcnt2^{-/-}$ (3), we assert that the most likely

explanation of the mitochondrial/metabolic phenotype in $Kcnt2^{-/-}$ hearts is loss of the channel from cardiac mitochondria.

The metabolic phenotype of $Kcnt2^{-/-}$ (Figs. 5 and 6) was manifest under conditions corresponding to classic bioenergetic “state 3,” wherein the mitochondrial membrane potential is consumed and generates ATP. If the *in situ* reversal potential of mitochondrial $K_{Na}1.2$ is above 0, then channel opening could readily occur under conditions of high energetic demand when potential is lowered. In addition, the mitochondrial membrane potential is known to flicker *in vivo* (53), such that transient depolarization events may activate mito- $K_{Na}1.2$. These properties may render mitochondrial $K_{Na}1.2$ function important under conditions of stress, such as tissue ischemia. Given the previously reported requirement of $K_{Na}1.2$ for cardioprotection by APC (3), it is notable that the mitochondrial membrane potential depolarizes and that cytosolic Na^+ levels also increase during ischemia (54, 55). Together, these observations suggest that mito- $K_{Na}1.2$ channels may be activated by acute perturbations in mitochondrial energy demand or under stress conditions, such as ischemia. Such properties may explain why the metabolic phenotype of $Kcnt2^{-/-}$ is evident only under stress.

A potential confounding factor in these studies was the use of BDM to inhibit contraction during the first stage only of cardiomyocyte isolation. BDM has been shown to affect ion channels including the K_V channels responsible for transient outward K^+ current I_{to} , Ca^{2+}/Na^+ exchanger, L-type Ca^{2+} channel, and skeletal muscle ryanodine receptor (56–59). However BDM's half-maximum inhibitory concentration for transient outward current and L-type Ca^{2+} channels are higher than the 10 mM used in our protocol, and the cardiac ryanodine receptor was found to be BDM insensitive. Although the half-maximum inhibitory concentration of Ca^{2+}/Na^+ exchanger for BDM was 2.4 mM, myocytes were successfully rendered Ca^{2+} tolerant and incubated in BDM-free medium after the first stage. As such, any effect of BDM on the channels being studied here is probably insignificant.

The data in Fig. 7 revealed additional chronic effects of $K_{Na}1.2$ loss on bioenergetics that resulted in altered body fat content and fasting glucose metabolism. Because of the presence of a mitochondrial K^+/H^+ exchanger, activation of a mitochondrial K^+ channel would be expected to decrease the mitochondrial ΔpH , thus uncoupling oxidative phosphorylation and stimulating OCR, as shown in Fig. 4B. Mild mitochondrial uncoupling by mito- $K_{Na}1.2$ channel activators may represent a novel therapeutic avenue for obesity/diabetes/metabolic syndrome. It is therefore notable that the antihelminthic drug niclosamide, which activates K_{Na} channels (60), has long been known to uncouple mitochondria (61) and was recently shown to confer benefits in a mouse high-fat diet model of diabetes (62). Furthermore, a recent case report highlighted a patient with a $K_{Na}1.2$ mutation ($Q_{270}E$) who had migrating focal seizures that were nonresponsive to the ketogenic diet typically used to treat such symptoms (63). Cardiac metabolomics also revealed a potential up-regulation of PLC signaling in the $Kcnt2^{-/-}$ heart (Fig.

8C). $K_{Na}1.2$ channels are known to interact with the PLC substrate PIP_2 (64), which raises the possibility that loss of $K_{Na}1.2$ results in perturbation of PIP_2 /PLC signaling. An important PLC downstream target is PKC_{ϵ} , which is known to play a role in development of insulin resistance in response to a high-fat diet (65). In addition to mitochondrial uncoupling, mito- $K_{Na}1.2$ channel activators may confer metabolic benefits *via* a PIP_2 /PLC/ PKC_{ϵ} signaling axis. A deeper investigation of the relationship between mito- $K_{Na}1.2$ activity and metabolic regulation is thus warranted. **FJ**

ACKNOWLEDGMENTS

The authors thank Christopher Lingle (Washington University, St. Louis, MO, USA) for providing founders for the *Kcnt2*^{-/-} mice; Kathleen Kinally (Emeritus, New York University, New York, NY, USA) for technical support in performing mitochondrial patch-clamp experiments; Dana Godfrey [University of Rochester Medical Center (URMC) Musculoskeletal Center] for support with the DEXA analyses; and Karen Bentley (URMC electron microscopy core) for support obtaining electron microscopic images. This work was funded by U.S. National Institutes of Health General Medical Research Grant R01-GM087483 (to P.S.B. and K.N.), National Heart, Lung and Blood Institute Grant R01-HL071158 (to P.S.B.), and National Institute of Arthritis and Musculoskeletal and Skin Diseases Grant R01-AR-059646 (to R.T.D.). The authors declare no conflicts of interest.

AUTHOR CONTRIBUTIONS

C. O. Smith, K. Nehrke, and P. S. Brookes designed the research; C. O. Smith, Y. T. Wang, S. M. Nadtochiy, and J. H. Miller performed the experiments; Y. T. Wang developed software for analysis of Langendorff traces; C. O. Smith analyzed the data; C. O. Smith and P. S. Brookes wrote the paper; and E. A. Jonas and R. T. Dirksen contributed new analytical tools, training, and critical resources.

REFERENCES

- Smith, C. O., Nehrke, K., and Brookes, P. S. (2017) The Slo(w) path to identifying the mitochondrial channels responsible for ischemic protection. *Biochem. J.* **474**, 2067–2094
- Bentzen, B. H., Nardi, A., Calloe, K., Madsen, L. S., Olesen, S. P., and Grunnet, M. (2007) The small molecule NS11021 is a potent and specific activator of Ca²⁺-activated big-conductance K⁺ channels. *Mol. Pharmacol.* **72**, 1033–1044
- Wojtovich, A. P., Smith, C. O., Urciuoli, W. R., Wang, Y. T., Xia, X. M., Brookes, P. S., and Nehrke, K. (2016) Cardiac Slo2.1 is required for volatile anesthetic stimulation of K⁺ transport and anesthetic preconditioning. *Anesthesiology* **124**, 1065–1076
- Garlid, K. D., Paucek, P., Yarov-Yarovsky, V., Murray, H. N., Darbenzio, R. B., D'Alonzo, A. J., Lodge, N. J., Smith, M. A., and Grover, G. J. (1997) Cardioprotective effect of diazoxide and its interaction with mitochondrial ATP-sensitive K⁺ channels. Possible mechanism of cardioprotection. *Circ. Res.* **81**, 1072–1082
- Inoue, I., Nagase, H., Kishi, K., and Higuti, T. (1991) ATP-sensitive K⁺ channel in the mitochondrial inner membrane. *Nature* **352**, 244–247
- Dolga, A. M., Netter, M. F., Perocchi, F., Doti, N., Meissner, L., Tobaben, S., Grohm, J., Zischka, H., Plesnila, N., Decher, N., and Culmsee, C. (2013) Mitochondrial small conductance SK2 channels

prevent glutamate-induced cytoxicity and mitochondrial dysfunction. *J. Biol. Chem.* **288**, 10792–10804

- Nabbi, R., Gadicherla, A. K., Kersten, J. R., Stowe, D. F., Lazar, J., and Riess, M. L. (2014) Genetically determined mitochondrial preservation and cardioprotection against myocardial ischemia-reperfusion injury in a consomic rat model. *Physiol. Genomics* **46**, 169–176
- Siemen, D., Loupatatzis, C., Borecky, J., Gulbins, E., and Lang, F. (1999) Ca²⁺-activated K channel of the BK-type in the inner mitochondrial membrane of a human glioma cell line. *Biochem. Biophys. Res. Commun.* **257**, 549–554
- Singh, H., Lu, R., Bopassa, J. C., Meredith, A. L., Stefani, E., and Toro, L. (2013) MitoBK(Ca) is encoded by the *Kcnma1* gene, and a splicing sequence defines its mitochondrial location [published correction in *Proc Natl Acad Sci* (2013) **110**, 18024]. *Proc. Natl. Acad. Sci. USA* **110**, 10836–10841
- Foster, D. B., Ho, A. S., Rucker, J., Garlid, A. O., Chen, L., Sidor, A., Garlid, K. D., and O'Rourke, B. (2012) Mitochondrial ROMK channel is a molecular component of mitoK(ATP). *Circ. Res.* **111**, 446–454
- Soltysinska, E., Bentzen, B. H., Barthmes, M., Hattel, H., Thrush, A. B., Harper, M. E., Qvortrup, K., Larsen, F. J., Schiffer, T. A., Losa-Reyna, J., Straubinger, J., Kniess, A., Thomsen, M. B., Brüggemann, A., Fenske, S., Biel, M., Ruth, P., Wahl-Schott, C., Boushel, R. C., Olesen, S. P., and Lukowski, R. (2014) KCNMA1 encoded cardiac BK channels afford protection against ischemia-reperfusion injury. *PLoS One* **9**, e103402
- Frankenreiter, S., Bednarczyk, P., Kniess, A., Bork, N., Straubinger, J., Koprowski, P., Wrzosek, A., Mohr, E., Logan, A., Murphy, M. P., Gawaz, M., Krieg, T., Szcwyczyk, A., Nikolaev, V. O., Ruth, P., and Lukowski, R. (2017) cGMP-elevating compounds and ischemic conditioning provide cardioprotection against ischemia and reperfusion injury via cardiomyocyte-specific BK channels. *Circulation* **136**, 2337–2355
- Calvo, S. E., Clauser, K. R., and Mootha, V. K. (2016) MitoCarta2.0: an updated inventory of mammalian mitochondrial proteins. *Nucleic Acids Res.* **44**(D1), D1251–D1257
- Joiner, W. J., Tang, M. D., Wang, L. Y., Dworetzky, S. I., Boissard, C. G., Gan, L., Gribkoff, V. K., and Kaczmarek, L. K. (1998) Formation of intermediate-conductance calcium-activated potassium channels by interaction of Slack and Slo subunits. *Nat. Neurosci.* **1**, 462–469
- Bhattacharjee, A., Joiner, W. J., Wu, M., Yang, Y., Sigworth, F. J., and Kaczmarek, L. K. (2003) Slick (Slo2.1), a rapidly-gating sodium-activated potassium channel inhibited by ATP. *J. Neurosci.* **23**, 11681–11691
- Kawasaki, Y., Kuki, I., Ehara, E., Murakami, Y., Okazaki, S., Kawawaki, H., Hara, M., Watanabe, Y., Kishimoto, S., Suda, K., Saito, H., and Matsumoto, N. (2017) Three cases of KCNT1 mutations: malignant migrating partial seizures in infancy with massive systemic to pulmonary collateral arteries. *J. Pediatr.* **191**, 270–274
- Gururaj, S., Palmer, E. E., Sheehan, G. D., Kandula, T., Macintosh, R., Ying, K., Morris, P., Tao, J., Dias, K. R., Zhu, Y., Dinger, M. E., Cowley, M. J., Kirk, E. P., Roscioli, T., Sachdev, R., Duffey, M. E., Bye, A., and Bhattacharjee, A. (2017) A de novo mutation in the sodium-activated potassium channel KCNT2 alters ion selectivity and causes epileptic encephalopathy. *Cell Reports* **21**, 926–933
- Martinez-Espinosa, P. L., Wu, J., Yang, C., Gonzalez-Perez, V., Zhou, H., Liang, H., Xia, X. M., and Lingle, C. J. (2015) Knockout of Slo2.2 enhances itch, abolishes KNa current, and increases action potential firing frequency in DRG neurons. *Elife* **4**, e10014
- Kameyama, M., Kakei, M., Sato, R., Shibasaki, T., Matsuda, H., and Irisawa, H. (1984) Intracellular Na⁺ activates a K⁺ channel in mammalian cardiac cells. *Nature* **309**, 354–356
- Yang, B., Gribkoff, V. K., Pan, J., Dagnagez, V., Dworetzky, S. I., Boissard, C. G., Bhattacharjee, A., Yan, Y., Sigworth, F. J., and Kaczmarek, L. K. (2006) Pharmacological activation and inhibition of Slack (Slo2.2) channels. *Neuropharmacology* **51**, 896–906
- Szabo, I., and Zoratti, M. (2014) Mitochondrial channels: ion fluxes and more. *Physiol. Rev.* **94**, 519–608
- Murphy, E., and Eisner, D. A. (2009) Regulation of intracellular and mitochondrial sodium in health and disease. *Circ. Res.* **104**, 292–303
- Nita, I. I., Hershinkel, M., Lewis, E. C., and Sekler, I. (2015) A crosstalk between Na⁺ channels, Na⁺/K⁺ pump and mitochondrial Na⁺ transporters controls glucose-dependent cytosolic and mitochondrial Na⁺ signals. *Cell Calcium* **57**, 69–75
- Bay, J., Kohlhaas, M., and Maack, C. (2013) Intracellular Na⁺ and cardiac metabolism. *J. Mol. Cell. Cardiol.* **61**, 20–27

25. Aittokallio, T. (2010) Dealing with missing values in large-scale studies: microarray data imputation and beyond. *Brief. Bioinform.* **11**, 253–264
26. Xia, J., and Wishart, D. S. (2016) Using metaboAnalyst 3.0 for comprehensive metabolomics data analysis. *Curr. Protoc. Bioinformatics* **55**, 14.10.1–14.10.91
27. Nadtochiy, S. M., Urciuoli, W., Zhang, J., Schafer, X., Munger, J., and Brookes, P. S. (2015) Metabolomic profiling of the heart during acute ischemic preconditioning reveals a role for SIRT1 in rapid cardioprotective metabolic adaptation. *J. Mol. Cell. Cardiol.* **88**, 64–72
28. Toledo-Arana, A., Dussurget, O., Nikitas, G., Sesto, N., Guet-Revillet, H., Balestrino, D., Loh, E., Gripenland, J., Tiensuu, T., Vaitkevicius, K., Barthelemy, M., Vergassola, M., Nahori, M. A., Soubigou, G., Régnault, B., Coppée, J. Y., Lecuit, M., Johansson, J., and Cossart, P. (2009) The *Listeria* transcriptional landscape from saprophytism to virulence. *Nature* **459**, 950–956
29. Szewczyk, A., Jarmuszkiwicz, W., and Kunz, W. S. (2009) Mitochondrial potassium channels. *IUBMB Life* **61**, 134–143
30. Dryer, S. E., Fujii, J. T., and Martin, A. R. (1989) A Na⁺-activated K⁺ current in cultured brain stem neurones from chicks. *J. Physiol.* **410**, 283–296
31. Kaczmarek, L. K. (2013) Slack, slick and sodium-activated potassium channels. *ISRN Neurosci.* **2013**, 1–14
32. Kim, G. E., Kronengold, J., Barcia, G., Quraishi, I. H., Martin, H. C., Blair, E., Taylor, J. C., Dulac, O., Colleaux, L., Nabbout, R., and Kaczmarek, L. K. (2014) Human slack potassium channel mutations increase positive cooperativity between individual channels. *Cell Reports* **9**, 1661–1672
33. Chen, H., Kronengold, J., Yan, Y., Gazula, V. R., Brown, M. R., Ma, L., Ferreira, G., Yang, Y., Bhattacharjee, A., Sigworth, F. J., Salkoff, L., and Kaczmarek, L. K. (2009) The N-terminal domain of Slack determines the formation and trafficking of Slick/Slack heteromeric sodium-activated potassium channels. *J. Neurosci.* **29**, 5654–5665
34. Kaczmarek, L. K., Aldrich, R. W., Chandry, K. G., Grissmer, S., Wei, A. D., and Wulff, H. (2017) International union of basic and clinical pharmacology. C. Nomenclature and properties of calcium-activated and sodium-activated potassium channels. *Pharmacol. Rev.* **69**, 1–11
35. Kim, G. E., and Kaczmarek, L. K. (2014) Emerging role of the KCNT1 Slack channel in intellectual disability. *Front. Cell. Neurosci.* **8**, 209
36. Garlid, K. D. (1996) Cation transport in mitochondria—the potassium cycle. *Biochim. Biophys. Acta* **1275**, 123–126
37. Bednarczyk, P., Wieckowski, M. R., Broszkiewicz, M., Skowronek, K., Siemen, D., and Szewczyk, A. (2013) Putative structural and functional coupling of the mitochondrial BKCa channel to the respiratory chain. *PLoS One* **8**, e68125
38. Checchetto, V., Teardo, E., Carraretto, L., Leanza, L., and Szabo, I. (2016) Physiology of intracellular potassium channels: a unifying role as mediators of counterion fluxes? *Biochim. Biophys. Acta.* **1857**, 1258–1266
39. Tejada, M. A., Hashem, N., Calloe, K., and Klaerke, D. A. (2017) Heteromeric Slick/Slack K⁺ channels show graded sensitivity to cell volume changes. *PLoS One* **12**, e0169914
40. Tejada, M. A., Stople, K., Hammami Bomholtz, S., Meinild, A. K., Poulsen, A. N., and Klaerke, D. A. (2014) Cell volume changes regulate slick (Slo2.1), but not slack (Slo2.2) K⁺ channels. *PLoS One* **9**, e110833
41. Picard, M., White, K., and Turnbull, D. M. (2013) Mitochondrial morphology, topology, and membrane interactions in skeletal muscle: a quantitative three-dimensional electron microscopy study. *J. Appl. Physiol.* **114**, 161–171
42. Bugger, H., Chen, D., Riehle, C., Soto, J., Theobald, H. A., Hu, X. X., Ganesan, B., Weimer, B. C., and Abel, E. D. (2009) Tissue-specific remodeling of the mitochondrial proteome in type 1 diabetic akita mice. *Diabetes* **58**, 1986–1997
43. Laskowski, M., Augustynek, B., Kulawiak, B., Koprowski, P., Bednarczyk, P., Jarmuszkiwicz, W., and Szewczyk, A. (2016) What do we not know about mitochondrial potassium channels? *Biochim. Biophys. Acta.* **1857**, 1247–1257
44. Testai, L., Rapposelli, S., Martelli, A., Breschi, M. C., and Calderone, V. (2015) Mitochondrial potassium channels as pharmacological target for cardioprotective drugs. *Med. Res. Rev.* **35**, 520–553
45. Ertracht, O., Malka, A., Atar, S., and Binah, O. (2014) The mitochondria as a target for cardioprotection in acute myocardial ischemia. *Pharmacol. Ther.* **142**, 33–40
46. Tano, J. Y., and Gollasch, M. (2014) Hypoxia and ischemia-reperfusion: a BiK contribution? *Am. J. Physiol. Heart Circ. Physiol.* **307**, H811–H817
47. Stowe, D. F., Gadicherla, A. K., Zhou, Y., Aldakkak, M., Cheng, Q., Kwok, W. M., Jiang, M. T., Heisner, J. S., Yang, M., and Camara, A. K. (2013) Protection against cardiac injury by small Ca(2+)-sensitive K(+) channels identified in guinea pig cardiac inner mitochondrial membrane. *Biochim. Biophys. Acta* **1828**, 427–442
48. Ponnalagu, D., and Singh, H. (2016) Anion channels of mitochondria. *Handb. Exp. Pharmacol.* **240**, 71–101
49. Leanza, L., Biasutto, L., Managò, A., Gulbins, E., Zoratti, M., and Szabò, I. (2013) Intracellular ion channels and cancer. *Front. Physiol.* **4**, 227
50. Yang, B., Desai, R., and Kaczmarek, L. K. (2007) Slack and Slick K(Na) channels regulate the accuracy of timing of auditory neurons. *J. Neurosci.* **27**, 2617–2627
51. Thomson, S. J., Hansen, A., and Sanguinetti, M. C. (2015) Identification of the intracellular Na⁺ sensor in Slo2.1 potassium channels. *J. Biol. Chem.* **290**, 14528–14535
52. Wojtovich, A. P., Sherman, T. A., Nadtochiy, S. M., Urciuoli, W. R., Brookes, P. S., and Nehrke, K. (2011) SLO-2 is cytoprotective and contributes to mitochondrial potassium transport. *PLoS One* **6**, e28287
53. O'Reilly, C. M., Fogarty, K. E., Drummond, R. M., Tuft, R. A., and Walsh, J. V., Jr. (2003) Quantitative analysis of spontaneous mitochondrial depolarizations. *Biophys. J.* **85**, 3350–3357
54. Green, D. R., and Kroemer, G. (2004) The pathophysiology of mitochondrial cell death. *Science* **305**, 626–629
55. Lesnefsky, E. J., Moghaddas, S., Tandler, B., Kerner, J., and Hoppel, C. L. (2001) Mitochondrial dysfunction in cardiac disease: ischemia-reperfusion, aging, and heart failure. *J. Mol. Cell. Cardiol.* **33**, 1065–1089
56. Xiao, Y. F., and McArdle, J. J. (1995) Activation of protein kinase A partially reverses the effects of 2,3-butanedione monoxime on the transient outward K⁺ current of rat ventricular myocytes. *Life Sci.* **57**, 335–343
57. Watanabe, Y., Iwamoto, T., Matsuoka, I., Ohkubo, S., Ono, T., Watano, T., Shigekawa, M., and Kimura, J. (2001) Inhibitory effect of 2,3-butanedione monoxime (BDM) on Na(+)/Ca(2+) exchange current in guinea-pig cardiac ventricular myocytes. *Br. J. Pharmacol.* **132**, 1317–1325
58. Eisfeld, J., Mikala, G., Varadi, G., Schwartz, A., and Klöckner, U. (1997) Inhibition of cloned human L-type cardiac calcium channels by 2,3-butanedione monoxime does not require PKA-dependent phosphorylation sites. *Biochem. Biophys. Res. Commun.* **230**, 489–492
59. Tripathy, A., Xu, L., Pasek, D. A., and Meissner, G. (1999) Effects of 2,3-butanedione 2-monoxime on Ca²⁺ release channels (ryanodine receptors) of cardiac and skeletal muscle. *J. Membr. Biol.* **169**, 189–198
60. Biton, B., Sethuramanujam, S., Picchione, K. E., Bhattacharjee, A., Khessibi, N., Chesney, F., Lanneau, C., Curet, O., and Arvenet, P. (2012) The antipsychotic drug loxapine is an opener of the sodium-activated potassium channel slack (Slo2.2). *J. Pharmacol. Exp. Ther.* **340**, 706–715
61. Weinbach, E. C., and Garbus, J. (1969) Mechanism of action of reagents that uncouple oxidative phosphorylation. *Nature* **221**, 1016–1018
62. Tao, H., Zhang, Y., Zeng, X., Shulman, G. I., and Jin, S. (2014) Niclosamide ethanolamine-induced mild mitochondrial uncoupling improves diabetic symptoms in mice. *Nat. Med.* **20**, 1263–1269
63. Madaan, P., Jauhari, P., Gupta, A., Chakrabarty, B., and Gulati, S. (2018) A quinidine non responsive novel KCNT1 mutation in an Indian infant with epilepsy of infancy with migrating focal seizures. *Brain Dev.* **40**, 229–232
64. De los Angeles Tejada, M., Jensen, L. J., and Klaerke, D. A. (2012) PIP₂ modulation of Slick and Slack K⁺ channels. *Biochem. Biophys. Res. Commun.* **424**, 208–213
65. Samuel, V. T., Liu, Z. X., Wang, A., Beddow, S. A., Geisler, J. G., Kahn, M., Zhang, X. M., Monia, B. P., Bhanot, S., and Shulman, G. I. (2007) Inhibition of protein kinase Cepsilon prevents hepatic insulin resistance in nonalcoholic fatty liver disease. *J. Clin. Invest.* **117**, 739–745

Received for publication January 24, 2018.

Accepted for publication May 7, 2018.